

# NAVAL POSTGRADUATE SCHOOL

## Monterey, California



### THESIS

**EXAMINATION OF TIME-REVERSAL ACOUSTICS IN  
SHALLOW WATER AND APPLICATIONS TO  
UNDERWATER COMMUNICATIONS**

by

António Adolfo Mendes Abrantes

June 1999

Thesis Advisors:

Kevin B. Smith  
Andrés Larraza  
Monique P. Fargues

Approved for public release; distribution is unlimited.

19990930 030

REPORT DOCUMENTATION PAGE			Form Approved OMB No. 0704-0188	
Public reporting burden for this collection of information is estimated to average 1 hour per response, including the time reviewing instructions, searching existing data sources, gathering and maintaining the data needed, and completing and reviewing the collection of information. Send comments regarding this burden estimate or any other aspect of this collection of information, including suggestions for reducing this burden to Washington Headquarters Services, Directorate for Information Operations and Reports, 1215 Jefferson Davis Highway, Suite 1204, Arlington, VA 22202-4302, and to the Office of Management and Budget, Paperwork Reduction Project (0704-0188), Washington, DC 20503.				
1. AGENCY USE (Leave Blank)		2. REPORT DATE June 1999		3. REPORT TYPE AND DATES COVERED Master's Thesis
4. TITLE AND SUBTITLE Examination of Time-Reversal Acoustics in Shallow Water and Applications to Underwater Communications			5. FUNDING NUMBERS	
6. AUTHOR(S) Antônio Adolfo Mendes Abrantes				
7. PERFORMING ORGANIZATION NAME(S) AND ADDRESS(ES) Naval Postgraduate School Monterey, CA 93943-5000			8. PERFORMING ORGANIZATION REPORT NUMBER	
9. SPONSORING / MONITORING AGENCY NAME(S) AND ADDRESS(ES)			10. SPONSORING / MONITORING AGENCY REPORT NUMBER	
11. SUPPLEMENTARY NOTES The views expressed in this thesis are those of the author and do not reflect the official policy or position of the Department of Defense or the United States Government.				
12a. DISTRIBUTION / AVAILABILITY STATEMENT Approved for public release; distribution is unlimited.			12b. DISTRIBUTION CODE	
13. ABSTRACT (Maximum 200 words) Time-varying multipath propagation is considered the most important difficulty in shallow underwater acoustic (UWA) communications. To compensate for the time variability of the channel, the receiver must use an adaptive algorithm for adjusting its parameters. At high symbol rates, intersymbol interference caused by multipath propagation requires large adaptive filters, increasing the computational complexity at the receiver end. This thesis presents a time-reversal acoustic technique (implemented with a phase-conjugated array or PCA) that generates a spatio-temporal focus of acoustic energy at the receiver location which reduces distortions introduced by channel propagation (including multipath), allowing the use of low-complexity receivers. Numerical analysis shows that for different PCA geometries (element spacing and aperture sizes), the PCA focus footprint does not appear to significantly change its dimensions. Furthermore, the aperture size plays a more significant role than the number of array elements in a PC array design. Specific examples of novel UWA communication systems utilizing time-reversal focusing are introduced. Current simulation results suggest the potential for high data transfer rates compared to existing noncoherent UWA communication systems.				
14. SUBJECT TERMS Underwater Acoustic Communications, Command, Control and Communications			15. NUMBER OF PAGES 91	
			16. PRICE CODE	
17. SECURITY CLASSIFICATION OF REPORT Unclassified	18. SECURITY CLASSIFICATION OF THIS PAGE Unclassified	19. SECURITY CLASSIFICATION OF ABSTRACT Unclassified	20. LIMITATION OF ABSTRACT Unlimited	

NSN 7540-01-280-5500

Standard Form 298 (Rev. 2-89)  
Prescribed by ANSI Std. Z39-18



Approved for public release; distribution is unlimited.

**EXAMINATION OF TIME-REVERSAL ACOUSTICS IN SHALLOW WATER  
AND APPLICATIONS TO UNDERWATER COMMUNICATIONS**

António Adolfo Mendes Abrantes  
Lieutenant, Portuguese Navy  
B. S., Escola Naval, 1993

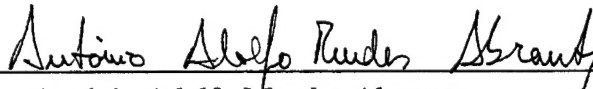
Submitted in partial fulfillment of the  
requirements for the degree of

**MASTER OF SCIENCE  
IN  
ENGINEERING ACOUSTICS AND ELECTRICAL ENGINEERING**

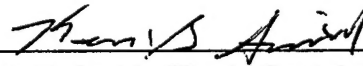
from the

**NAVAL POSTGRADUATE SCHOOL  
June 1999**

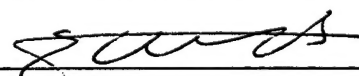
Author:

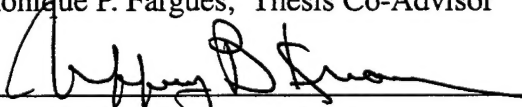
  
António Adolfo Mendes Abrantes

Approved by:

  
Kevin B. Smith, Thesis Co-Advisor, Chairman  
Engineering Acoustics Academic Committee

  
Andrés Larraza, Thesis Co-Advisor

  
Monique P. Fargues, Thesis Co-Advisor

  
Jeffrey B. Knorr, Chairman  
Department of Electrical and Computer Engineering





## ABSTRACT

Time-varying multipath propagation is considered the most important difficulty in shallow underwater acoustic (UWA) communications. To compensate for the time variability of the channel, the receiver must use an adaptive algorithm for adjusting its parameters. At high symbol rates, intersymbol interference caused by multipath propagation requires large adaptive filters, increasing the computational complexity at the receiver end.

This thesis presents a time-reversal acoustic technique (implemented with a phase-conjugated array of PCA) that generates a spatio-temporal focus of acoustic energy at the receiver location which reduces distortions introduced by channel propagation (including multipath), allowing the use of low-complexity receivers. Numerical analysis shows that for different PCA geometries (element spacing and aperture sizes), the PCA focus footprint does not appear to significantly change its dimensions. Furthermore, the aperture size plays a more significant role than the number of array elements in a PC array design.

Specific examples of novel UWA communication systems utilizing time-reversal focusing are introduced. Current simulation results suggest the potential for high data transfer rates compared to existing noncoherent UWA communication systems.



## TABLE OF CONTENTS

I.	INTRODUCTION .....	1
II.	TIME REVERSAL ACOUSTICS THEORY	11
A.	OVERVIEW OF TIME REVERSAL ACOUSTICS THEORY .....	11
B.	TIME REVERSAL IN A RANGE-INDEPENDENT UNDERWATER ACOUSTIC CHANNEL .....	18
C.	TIME REVERSAL ACOUSTICS IN A STATIC RANGE- DEPENDENT UNDERWATER ACOUSTIC CHANNEL .....	19
III.	NUMERICAL MODELING OF THE TIME-REVERSAL ARRAY .....	23
A.	PARABOLIC EQUATION THEORY .....	23
B.	PARABOLIC EQUATION NUMERICAL SOLUTION .....	27
C.	MONTEREY-MIAMI PARABOLIC EQUATION MODELING .....	28
D.	TIME ARRIVAL STRUCTURE .....	29
E.	TIME DOMAIN ANIMATION OF SPATIAL ACOUSTIC PROPAGATION .....	31
IV.	ENVIRONMENTAL INFLUENCES ON TIME-REVERSAL ACOUSTICS .....	33
A.	ENVIRONMENT CHARACTERIZATION .....	34
B.	TRANSMITTED SIGNAL ENVELOPE .....	35
C.	TIME REVERSAL ACOUSTICS IN A RANGE-INDEPENDENT ENVIRONMENT .....	35
D.	FOCUSING AT DIFFERENT FREQUENCIES .....	42
E.	CHANNEL CHARACTERIZATION IN THE FREQUENCY DOMAIN .....	43
F.	EFFECT OF INTER-ELEMENT SPACING .....	45
G.	EFFECT OF APERTURE SIZE .....	47
H.	EFFECT OF FREQUENCY BIN SHIFTING ON FOCUSING AT OTHER LOCATIONS IN RANGE .....	49
V.	APPLICATION OF TIME REVERSAL ACOUSTICS TO SHALLOW WATER COMMUNICATION SYSTEMS .....	53
A.	USING PHASE-CONJUGATED ARRAYS IN UNDERWATER ACOUSTIC COMMUNICATIONS .....	53
B.	SIGNALING SCHEME .....	56
C.	PHASE-CONJUGATED ARRAY .....	57
D.	POINT TO POINT MESSAGE TRANSMISSION .....	59
E.	PHASE CONJUGATED-ARRAY VERTICAL DENSITY IN UNDERWATER COMMUNICATIONS .....	61
F.	PHASE-CONJUGATED ARRAY SPATIAL DIVERSITY IN UNDERWATER COMMUNICATIONS .....	65

VI. CONCLUSIONS .....	71
LIST OF REFERENCES .....	75
INITIAL DISTRIBUTION LIST .....	79

## LIST OF FIGURES

1.1.	Single Pulse Propagation in a Shallow Water Channe.....	5
1.2.	Transmitted Signal Spectrum (First Panel), Transmitted Signal Envelope (Second Panel), Transmitted Signal in Time Domain (Third Panel) and Received Signal on a Single Array Element at Range 6km from the Source and Depth 150m (Lower Panel).....	6
1.3.	Time-Reversed Propagation from the PCA .....	7
2.1.	Waveguide Theory .....	11
2.2.	Multipath Arrival at Array Element.....	13
2.3.	Time Reversal Propagation .....	13
4.1.	UWA Channel Profile .....	34
4.2.	Transmitted Signal Envelope .....	36
4.3.	Ocean Response at 800Hz .....	36
4.4.	Time Arrival Structure at the PCA .....	37
4.5.	Envelope Cross-Correlation across the Array Elements.....	38
4.6.	Backward Propagation Ocean Response at 800Hz.....	39
4.7.	Time Arrival Structure Focus Range. Temporal, Vertical and Horizontal PCA Focusing Properties.....	41
4.8.	Focusing at Different Frequencies .....	42
4.9.	Forward Propagation Channel Frequency Response at the PC Array Element Located 150m Deep .....	43
4.10.	TwoWay Channel Frequency Response at Focus Location .....	44
4.11.	Focusing Properties Using PC Arrays with Different Element Spacing .....	46
4.12.	Focusing Properties Using PC Arrays with Different Aperture Size .....	48
4.13.	Focus Range Shifting by Changing the Carrier Frequency at PCA .....	50
4.14.	Focus Range Shifting for a Source 50m Deep.....	51
4.15.	Focus Range Shifting for a Source 100m Deep.....	52
5.1.	Channel Geometry in a Point to Point Communication Link.....	54
5.2.	PCA Element Filter Bank Frequency Response .....	58
5.3.	Spectrogram of the Signal Containing the Desired Message if no Distortions are Present in the Channel.....	60
5.4.	Message Signal Spectrogram Received by a Single Element Receiver 150m Deep, Evaluated at the PCA (Upper Left), at Two Intermediate Ranges and at the Focus (Lower Right) .....	60
5.5.	PCA Geometry for Vertical Diversity Examination .....	61
5.6.	Desired Message Signals for Node 2 Receivers .....	63
5.7.	Transmitted Signal by PCA 1 and Received Signals at Node 2 Receivers...64	
5.8.	Received Signal Spectrogram at Depth of 150m and Different Ranges from PCA 1 .....	64
5.9.	PCA 1 Geometry for Examination of Vertical and Horizontal Spatial Diversity in a UWA Communication Network.....	65
5.10.	Desired Signals to Focus at the Receivers .....	67
5.11.	Received Signal Spectrogram at the Receivers .....	68

5.12. Received Signal Spectrogram at a Depth of 150m and Different Ranges from Node 1 .....	69
--	----

## I. INTRODUCTION

Traditionally, applications for underwater acoustic (UWA) communication systems were almost exclusively military. In the last 10 years there has been a growing need of UWA communication systems for commercial applications. As a consequence, there was a tremendous increase in research and development of UWA communication systems. Applications that have received much attention lately are secure military communications, pollution monitoring, remote control in off-shore oil industry, video telemetry (using camera images or side scan sonar images from remotely operated vehicles) and collection of scientific data recorded at benthic stations without the need for retrieving the instruments. Many of the applications being developed are now calling for near real-time communication with submarines and remotely operated vehicles. As the UWA communications channel has limited bandwidth available, the bandwidth efficiency becomes an important issue for a UWA communication system.

The shallow water acoustic communication channel is characterized by strong signal degradation caused by multipath propagation and high spatial and temporal variability of the channel conditions. In any underwater acoustic environment there is limited bandwidth available due to transmission loss which increases with both frequency and range. This is a major constraint in underwater communication systems design. The most important of the difficulties encountered in shallow water acoustics digital communications is considered to be the time-varying multipath propagation (Catipovic, 1990, Baggeroer, 1984 and Coates et al., 1993). This leads to a requirement for powerful and reliable receiver algorithms for signal processing in a shallow water environment. In



recent years there was a large effort made in the design of techniques and algorithms to overcome this problem.

In a digital communication system, multipath propagation causes intersymbol interference (ISI). As an example, in a medium-range, 6km long, shallow water (200m) channel, a typical value for multipath delay spread is 30ms. If the communication system is signaling at 1 kilosymbol per second, the ISI will extend over 30 symbols, making it difficult for a receiver to recover the original message.

In shallow waters, multipath is primarily due to reflections at the surface and bottom of the channel. The multipath structure depends on the channel geometry, frequency of transmitted signals and on the source and receiver locations. On a small time scale, the most important contribution to channel variability is surface scattering due to waves producing time-varying multipaths. On a larger time scale, channel variation is due to a variety of effects including internal waves, temperature gradients, and currents in the sound speed profile.

The ISI and strong phase fluctuations caused by multipath propagation and temporal channel variability have in the past led to system designs based exclusively on noncoherent detection methods. These systems have poor spectral efficiency and low signaling rates and are still in use when robustness is the principal requirement in system design. To overcome the problem of ISI these systems employ signal design with guard times which are inserted between consecutive pulses to ensure that all the reverberation will vanish before each subsequent pulse is to be received (Stojanovic, 1996). The insertion of guard times obviously results in a reduction of the available data throughput.

In recent years, the feasibility of bandwidth-efficient phase-coherent modulation techniques for UWA communications has been proven (Stojanovic et al., 1993, Stojanovic et al., 1994, and Stojanovic et al., 1995). Several systems have been proposed and implemented using differential and purely coherent detection methods resulting in increased data throughput. In order to accommodate higher signaling rates, these systems must allow for ISI in the received signal and be able to track any phase variations due to changing channel conditions. In order to compensate for the ISI these systems employ either some form of array processing, for exploitation of spatial diversity, or equalization or a combination of both.

Array processing for multipath suppression has been used both at the transmitter end and at the receiver end. Coates (1993) and Galvin and Coates (1994), describe an approach that uses transmitter arrays to excite only a single path of propagation. Long arrays and careful positioning are required to ensure complete absence of multipath. In general it was found that this technique is more effective at shorter ranges.

Another approach (Howe et al., 1994, Tarbit et al., 1994, and Henderson et al., 1994) is based on adaptive beamforming at the receiver end. It uses a least mean squares (LMS) type of algorithm to adaptively steer nulls in the direction of a surface reflected wave. It was found to decrease in performance as the range increases in relation to depth (Tarbit et al., 1994). In order to complement the performance of the beamformer, an equalizer was proposed by Howe et al. (1994). The equalizer is of a decision-feedback type and operates under an LMS algorithm whose low computational requirements allow real-time adaptation at the symbol rate.

A different approach based on purely phase-coherent detection methods is described by Stojanovic et al. (1993, 1994 and 1995). The signal processing methods are based on joint synchronization and equalization to counter the effect of phase variations and ISI. It incorporates spatial signal processing based on combining diversity and a fractionally-spaced decision-feedback equalization with a recursive least squares (RLS) algorithm.

The channel distortions encountered in the underwater acoustic channel require complex receiver structures resulting in high computational requirements which may exceed the speeds of available hardware. In order to compensate for the time variability of the channel, the receiver must use an adaptive algorithm for adjusting its parameters based on a beamforming, equalization or combined approach. At high symbol rates, the long ISI requires large adaptive filters therefore increasing the computational complexity.

The aim of the present thesis is to provide an original and elegant solution to compensate for the distortions of the shallow water channel. This solution is not based on sophisticated processing algorithms but is equivalent to matched field processing with the filter matched to the impulse response of the ocean. The low computational load required in this technique is due to the fact that it uses the ocean itself as the matched filter for the acoustic propagation between source and receiver. By using rather simple signal processing at the transmitter (suitable for real-time implementation) the multipath structure at the receiver end is virtually absent, allowing a reduced-complexity receiver structure.

This technique uses time-reversal acoustic (TRA) arrays to generate a spatio-temporal focus of acoustic energy at the receiver location eliminating distortions introduced by channel propagation (Abrantes et al., 1999). Throughout this thesis the Monterey-Miami

Parabolic Equation (MMPE) acoustic propagation model (Smith and Tappert, 1994) is used for time-reversal acoustics numerical modeling. Figures 1.1, 1.2 and 1.3 present numerical modeling results of an acoustic pulse propagation from the source to the time-reversal array (forward propagation) and the propagation from the time-reversal array to the source (backward propagation). Figure 1.1 illustrates single pulse propagation from a

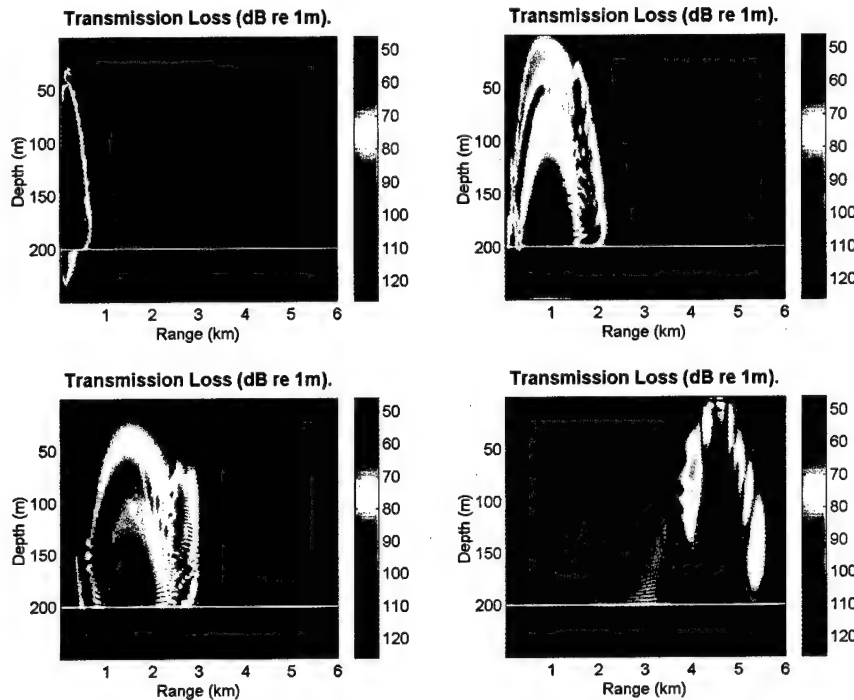


Figure 1.1. Single Pulse Propagation in a Shallow Water Channel.

source located 150m deep at the origin to a vertical array 6km away. Figure 1.2 illustrates the transmitted signal features and the multipath arrival structure of the recorded signal by the 150m deep array element. As seen in Figure 1.2 the transmitted pulse envelope has a -3dB temporal width of 14.1ms. It has a carrier frequency of 800Hz and its spectrum has a -3dB bandwidth of 36.6Hz. The transmitted pulse spectrum is given by the normalized coefficients of a Hanning window spanning 100Hz about the carrier frequency. The

complete description of this range-independent channel can be found in Section 4.A, p.

34.

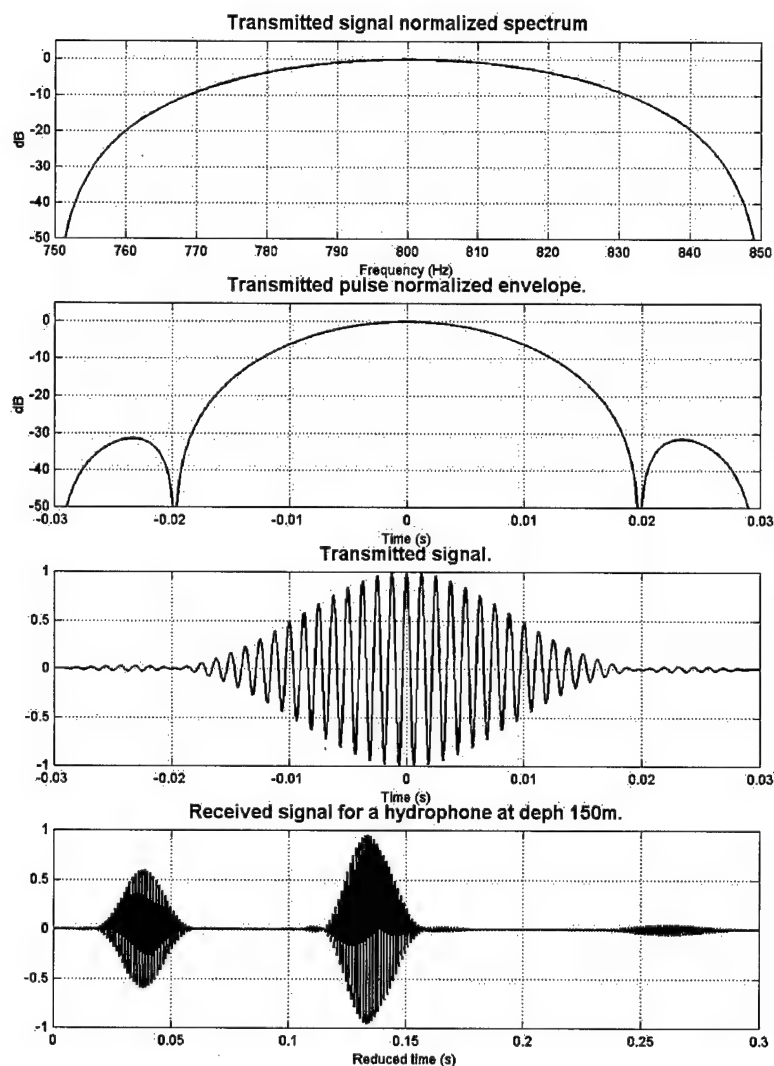


Figure 1.2. Transmitted Signal Spectrum (First Panel), Transmitted Signal Envelope (Second Panel), Transmitted Signal in Time Domain (Third Panel) and Received Signal on a Single Array Element at Range 6km from the Source and Depth 150m (Lower Panel).

In a time-reversal acoustic system, the distorted wavefield is recorded by the array, then transmitted in a time-reversed fashion (last signal recorded becomes the first transmitted). The time-reversed wavefield generated by the array propagates through the

medium and optimally focuses at the original source location. Note that the time-reversal process at the array is equivalent to a phase conjugation in the frequency domain. For this reason, the TRA array may also be referred to as the phase-conjugation array (PCA).

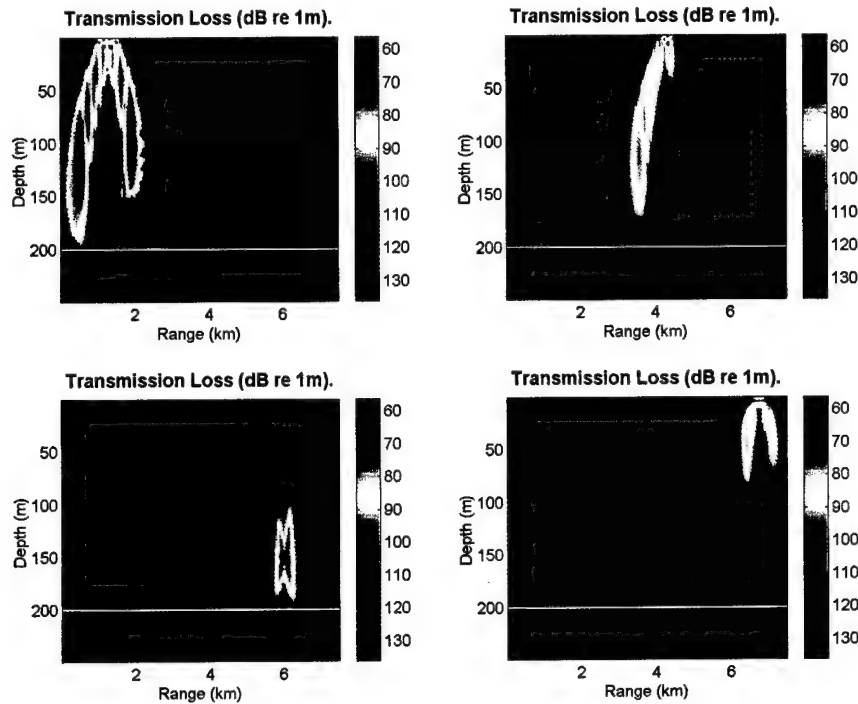


Figure 1.3. Time-Reversed Propagation from the PCA.

Figure 1.3 represents four snap-shots of the wavefield propagation from the PCA to the source. The spatial focusing at the source location is clearly observable in the lower left panel.

This technique can be considered a self-adaptive process that automatically compensates for any distortions due to propagation in the channel as well as any PCA imperfections. Clearly, due to the time-reversal transformation at the PCA, the received signal has the time-reversal signature of the signal which was transmitted originally. For

example, a linear up-sweep frequency modulated pulse will appear as a down-sweep at the focus.

This phase-conjugation process takes advantage of spatial reciprocity which is a property of wave propagation in a medium with stable refractive index. An acoustic phenomenon is said to satisfy spatial reciprocity if interchanging the positions of source and receiver does not alter the resulting wavefield at the receiver (Jensen et al., 1994). In general, reciprocity requires a static environment. TRA focusing requires spatial reciprocity in order to construct the exact time-reversed wavefield that will focus at the original source location. In this way, all the PCA elements transmit back to the source in a reciprocal fashion, and the time reversed wavefield will have the multipath structure undone at the source location.

Since the PCA only “learns” the medium structure that is imprinted in the incoming signal at the instant of its reception, it cannot compensate for refractive fluctuations that occur after reception of the signal. Also, if the environment or its boundaries change (due to surface waves, internal waves, temperature gradients, receiver or PCA motion, etc.), reciprocity is violated and the focusing properties of the PCA are degraded. To accommodate for temporal changes in the channel, the PCA must update the transfer function of the environment with some periodicity that depends on how fast environmental changes affect the focusing properties.

The remainder of this thesis consists of five chapters. Chapter II presents an overview of time reversal acoustics theory. In particular it analyses the cases of time reversal acoustics in a range-independent channel and a more general static range-dependent channel. In these ideal situations a closed-form solution for the field at the focus can be

evaluated, and some focusing properties can be inferred and may be extrapolated for more general environments. Chapter III presents an overview of the Monterey-Miami Parabolic Equation (MMPE) acoustic propagation model (Smith, 1996). This is the acoustic propagation model used throughout this thesis for time reversal acoustics numerical modeling. In Chapter IV the focusing properties of the PCA are studied through MMPE numerical simulations. It shows how the PCA focusing properties change when the array operates at different carrier frequencies, and when the array length or the array element spacing is altered. It also presents the frequency characterization of the channel and gives examples of how range shifting of the focus location can be attained. Chapter V describes applications of PC arrays to UWA communications and Chapter VI presents a summary of conclusions and identifies some aspects of PCA modeling requiring further research.





## II. TIME REVERSAL ACOUSTICS THEORY

This chapter presents an overview of time reversal acoustics (TRA) theory and its close relationship to matched field processing techniques. In particular it shows a closed form solution of the focus field in a simple range-independent environment. It also makes a generalization for a static range-dependent environment where an approximation of the field at the focus location can be evaluated. From this approximation the focusing properties of PC arrays can be evaluated.

### A. OVERVIEW OF TIME REVERSAL ACOUSTICS THEORY

For simplicity, consider a waveguide with pressure-release surface and rigid bottom as depicted in Figure 2.1 where the axis from  $o'$  to  $o$  will be the reference axis for

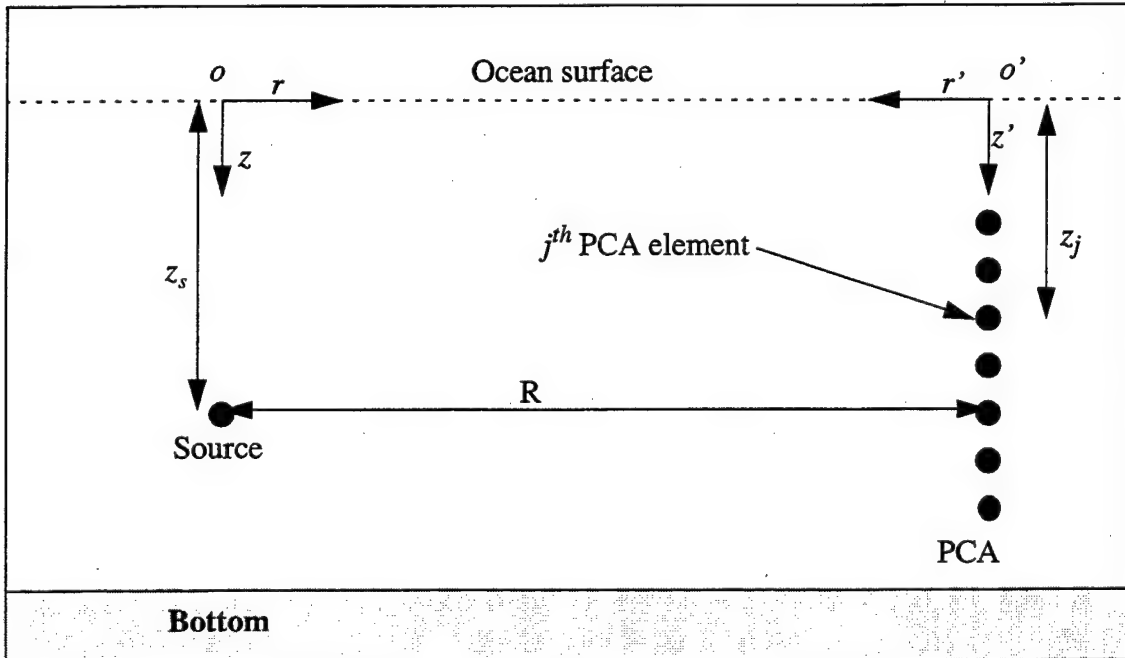


Figure 2.1. Waveguide Geometry.

propagation from the receiver array to the source. From the axis location in Figure 2.1 the

coordinates are related by  $z'=z$  and  $r'=R-r$ . In this environment the frequency-domain wave equation, or Helmholtz equation for a range-independent waveguide can be written as (Jensen et al., 1994)

$$[\nabla^2 + k^2(z)]G(r, z|z_s, \omega) = -\delta(r)\delta(z - z_s), \quad (2.1)$$

where  $k^2(z) = \frac{\omega^2}{c^2(z)}$  is the acoustic wavenumber for a waveguide with sound speed  $c(z)$ ,  $\omega$  denotes the angular frequency and  $G(r, z|z_s, \omega)$  is the frequency dependent Green's function in cylindrical coordinates at location  $(r, z)$  due to a point source located at range  $r = 0$  and depth  $z = z_s$ . Note that the depth  $z$  is taken positive downward.

From the point of view of linear systems theory, at location  $(r, z)$  the Green's function  $G(r, z|z_s, \omega)$  represents the ocean impulse response due to a point source located at range  $r = 0$  and depth  $z = z_s$ . It can be shown (Jensen et al., 1994) that  $G(r, z|z_s, \omega)$  satisfies the *principle of reciprocity*,

$$\rho(\vec{r}_s)G(\vec{r}_j|\vec{r}_s, \omega) = \rho(\vec{r}_j)G(\vec{r}_s|\vec{r}_j, \omega), \quad (2.2)$$

that is, the acoustic field measured at  $\vec{r}_j$  due to a point source located at  $\vec{r}_s$  is equal to the acoustic field that would be measured at  $\vec{r}_s$  if the point source were located at  $\vec{r}_j$  scaled by the ratio of densities at  $\vec{r}_s$  and  $\vec{r}_j$ . Since the density is nearly constant throughout the ocean, this leads to reciprocity of the acoustic field itself.

The reciprocity theorem plays a major role in time reversal acoustics because it implies that the field from an array element propagates to the source location in a reciprocal way as the field from the source to the array element. The acoustic field

recorded by a given array element has imprinted on it all the channel effects including multipath. Due to multipath propagation the signal recorded by a given PCA element will have multiple arrivals. Figure 2.2 illustrates the multipath arrival at a given PCA element

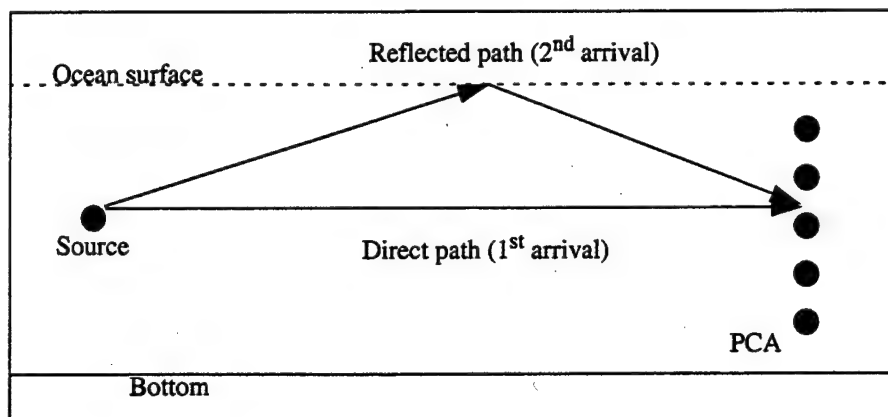


Figure 2.2. Multipath Arrival at Array Element.

where the direct path will arrive first and the reflected path will arrive second. After reception and recording, the received signal is time-reversed and transmitted back to the source. The back propagation from the array element to the source is illustrated in Figure 2.3. The travel times along the reciprocal paths will be the same, and so the multiple

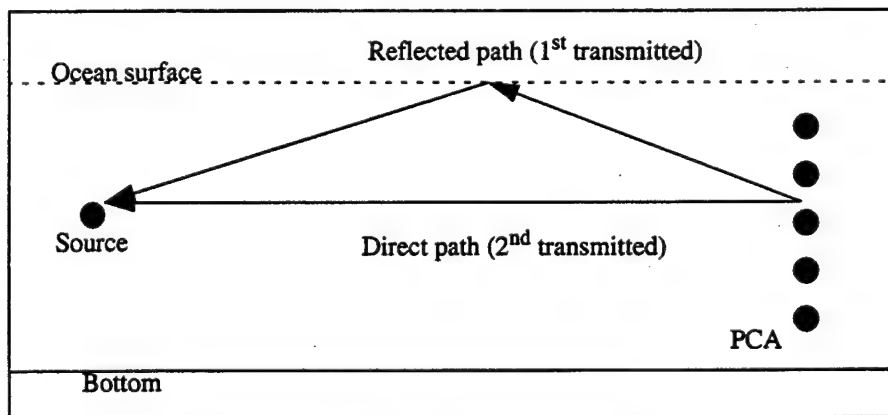


Figure 2.3. Time Reversal Propagation.

arrivals will arrive simultaneously back at the source location. Thus, at the source location the multipath structure will be undone.

At this point it should be mentioned that the term “time reversal” is used in reference to the time-reversal of the recorded signals performed at the PCA. It does not imply time-reversal of the waveguide effects because there is no way to reverse propagation losses in the channel transmission. Also, “phase conjugation” is synonymous with time-reversal at the array because of the time-reversal property of the Fourier transform. For a real signal one can write  $F[s(t)] = S(\omega)$ , where  $F[s(t)]$  denotes the Fourier transform of  $s(t)$ . Thus, the Fourier transform of the time-reversed signal  $s(-t)$  is then given by  $F[s(-t)] = S(-\omega) = S^*(\omega)$ . Therefore the time-reversal transformation is equivalent to complex conjugation in the frequency domain.

Due to the range-independent nature of the waveguide, a separation of variables technique may be used to solve the wave equation, Eq. (2.1). The solutions are then defined in terms of depth-dependent eigenfunctions, or normal modes, and range-dependent Hankel functions. In this situation, the azimuthally symmetric solutions have a far-field approximation given by (Jensen et al., 1994)

$$G(r, z|z_s, \omega) = \frac{i}{\rho(z_s)\sqrt{8\pi r}} e^{(-i\frac{\pi}{4})} \sum_{m=1}^{\infty} \Psi_m(z_s) \Psi_m(z) \frac{e^{iK_m r}}{\sqrt{K_m}}, \quad (2.3)$$

where  $r$  is the horizontal distance from the source,  $G(r, z|z_s, \omega)$  is the pressure field at location  $(r, z)$  due to a point source at  $z_s$ , scaled such that the pressure is unity at  $r=1m$ , and  $\Psi_m(z)$  and  $K_m$  are the normal mode eigenfunctions and modal wavenumbers, respectively.

The eigenfunctions and modal wavenumbers are obtained by solving the eigenvalue problem (Jensen et al., 1994)

$$\rho(z) \frac{d}{dz} \left[ \frac{1}{\rho(z)} \frac{d}{dz} \Psi_m(z) \right] + [k^2(z) - K_m^2] \Psi_m(z) = 0. \quad (2.4)$$

The mode functions  $\Psi_m(z)$  are orthogonal and normalized according to

$$\int_0^\infty \frac{\Psi_m(z) \Psi_n(z)}{\rho(z)} dz = \delta_{mn}, \quad (2.5)$$

and form a complete set (Kuperman et al., 1998),

$$\sum_{m=1}^\infty \frac{\Psi_m(z) \Psi_m(z_s)}{\rho(z_s)} = \delta(z - z_s). \quad (2.6)$$

When the source transmits a pulse  $s(t)$ , upon reception the  $j^{th}$  element of the PCA records the time-domain signal

$$p(R, z_j, t) = \int G(R, z_j | z_s, \omega) S(\omega) e^{-i\omega t} d\omega, \quad (2.7)$$

where  $S(\omega)$  is the Fourier transform of  $s(t)$  and  $R$  is the distance from the source to the PCA. Due to  $G(R, z_j | z_s, \omega)$ , the ocean impulse response, this equation incorporates all the waveguide effects including time elongation due to multipath propagation. For causality considerations, assume that the received signal  $p(R, z_j, t)$  lies in the interval  $0 < t < \tau$ , where  $\tau$  is large enough to include all multipath arrivals. In order to maintain causality the time reversed signal used to excite the  $j^{th}$  element of the PCA is  $p(R, z_j, T - t)$  where  $T$  is such that  $T > 2\tau$ . Under these considerations the time-reversed signal becomes

$$p(R, z_j, T-t) = \int_{-\infty}^{\infty} G(r, z_j|z_s, \omega) S(\omega) e^{-i\omega(T-t)} d\omega. \quad (2.8)$$

Using the conjugate symmetry of the transmitted pulse, i.e.,  $S(-\omega) = S^*(\omega)$ , and that of Green's function, i.e.,  $G(r, z_j|z_s, -\omega) = G^*(r, z_j|z_s, \omega)$ , and reversing the sign of the integration variable  $\omega$ , Eq. (2.8) comes

$$\begin{aligned} p(R, z_j, T-t) &= \int_{\infty}^{-\infty} G(r, z_j|z_s, -\omega) S(-\omega) e^{i\omega T} e^{-i\omega t} (-d\omega). \\ &= \int_{-\infty}^{\infty} [G^*(r, z_j|z_s, \omega) S^*(\omega) e^{i\omega T}] e^{-i\omega t} d\omega \end{aligned} \quad (2.9)$$

where the quantity in brackets is the Fourier transform of the signal transmitted by the  $j^{th}$  element of the PCA. This corresponds to the signal received by the element after time-reversal and delay. From Eq. (2.9) it becomes clear that the time reversal transformation is equivalent to complex conjugation in the frequency-domain plus a phase factor to observe causality.

Upon transmission back towards the source, the time reversed acoustic field  $P_{TRA}(r', z|z_j, \omega)$  generated by the  $j^{th}$  element of the PCA is given by

$$P_{TRA}(r', z|z_j, \omega) = G(r', z|z_j, \omega) G^*(R, z_j|z_s, \omega) S^*(\omega) e^{i\omega T}, \quad (2.10)$$

where  $G(r', z|z_j, \omega)$  is the field at location  $(r', z)$  due to a point source located at the  $j^{th}$  element of the PCA. The total field at  $(r', z)$  is given by the superposition of the field produced by each individual array element,

$$P_{TRA}(r', z|\omega) = \sum_{j=1}^J G(r', z|z_j, \omega) G^*(R, z_j|z_s, \omega) S^*(\omega) e^{i\omega T}. \quad (2.11)$$

By Fourier synthesis, the time-domain signal becomes

$$P_{TRA}(r', z, t) = \sum_{j=1}^J \int G(r', z|z_j, \omega) G^*(R, z_j|z_s, \omega) S^*(\omega) e^{i\omega T} e^{-i\omega t} d\omega. \quad (2.12)$$

At the source location  $r'=R$ , this expression becomes

$$P_{TRA}(R, z_s, t) = \sum_{j=1}^J \int G(R, z_s|z_j, \omega) G^*(R, z_j|z_s, \omega) S^*(\omega) e^{i\omega T} e^{-i\omega t} d\omega. \quad (2.13)$$

Using the reciprocity principle, Eq. (2.2), with constant density  $\rho(R, z_s) = \rho(R, z_j)$ , leads to

$$G(R, z_s|z_j, \omega) = G(R, z_j|z_s, \omega). \quad (2.14)$$

Therefore the time-domain equivalent of Eq.(2.13) is given by (Kuperman et al., 1998)

$$P_{TRA}(R, z_s, t) = \quad , \quad (2.15)$$

$$\frac{1}{(2\pi)^2} \int \left( \sum_{j=1}^J \left[ \int g_{t'+t''}(R, z_s|z_j, \omega) g_{t'}(R, z_s|z_j, \omega) dt' \right] s(t'' - t + T) \right) dt''$$

where  $g_{t'+t''}(R, z_s|z_j)$ ,  $g_{t'}(R, z_s|z_j)$  and  $s(t'' - t + T)$  are the time-domain representations of the Green's function and the probe signal.



The following observations can be made about Eq. (2.15) (Kuperman et al., 1998):

- The auto-correlation of the Green's function corresponds to a matched filtering operation with the filter matched to the impulse response of the propagation from the source to the  $j^{th}$  element of the array. This operation reduces the time elongation due to multipath propagation, producing a form of temporal focusing.
- It can be shown that the sum over the array elements is a form of spatial matched filtering analogous to that employed in the Bartlett matched field processor (Baggeroer et al., 1993).
- The sum over the array elements further improves temporal focusing as the side-lobes of the matched filters for each array element tend to average to zero which is also analogous to broadband matched-field processing results (Brienzo and Hodgkiss, 1993).
- The integral over  $t''$  is a convolution of each matched-filtered channel impulse response with the time-reversed and delayed transmitted pulse. As a consequence this pulse is not matched-filtered because a time-reversed version of it is received.

## B. TIME REVERSAL IN A RANGE-INDEPENDENT UNDERWATER ACOUSTIC CHANNEL

In order to evaluate the vertical focusing properties of the PCA, consider a range-independent channel where a closed-form solution for the field at the source can be evaluated. In a range-independent UWA channel the TRA field at location  $(r', z)$  can be found by substituting Eq. (2.3) into Eq. (2.12), such that

$$P_{TRA}(r', z, \omega) = \frac{S^*(\omega)e^{i\omega T}}{\rho(z_s)8\pi\sqrt{Rr'}} \sum_j \sum_m \sum_n \frac{\Psi_m(z)\Psi_m(z_j)\Psi_n(z_s)\Psi_n(z_j)}{\rho(z_j)\sqrt{K_m K_n}} e^{i(K_m r' - K_n R)}. \quad (2.16)$$

For an array that adequately samples all the modes, the summation over the PCA elements can be approximated by an integral

$$P_{TRA}(r', z, \omega) \equiv S^*(\omega) e^{i\omega T} \sum_m \sum_n \frac{\Psi_m(z) \Psi_n(z_s) e^{i(K_m r - K_n R)}}{\rho_{(z_s)} \delta\pi \sqrt{Rr'} \sqrt{K_m K_n}} \int_0^\infty \frac{\Psi_m(z) \Psi_n(z)}{\rho_{(z)}} dz. \quad (2.17)$$

Using the orthogonality property of the modes, Eq. (2.17) becomes

$$P_{TRA}(r', z, \omega) \equiv S^*(\omega) e^{i\omega T} \sum_m \frac{\Psi_m(z) \Psi_m(z_s) e^{iK_m(r' - R)}}{\rho_{(z_s)} \delta\pi K_m \sqrt{Rr'}}. \quad (2.18)$$

Evaluating Eq. (2.18) at the source range,  $r' = R$ , yields

$$P_{TRA}(R, z, \omega) \equiv S^*(\omega) e^{i\omega T} \sum_m \frac{\Psi_m(z) \Psi_m(z_s)}{\rho_{(z_s)} \delta\pi R K_m}. \quad (2.19)$$

Finally, assuming that  $K_m$  is nearly constant over the contributing modes and using the modal closure relation Eq. (2.6),

$$P_{TRA}(R, z, \omega) \equiv \frac{S^*(\omega) e^{i\omega T}}{\delta\pi R K} \sum_m \frac{\Psi_m(z) \Psi_m(z_s)}{\rho_{(z_s)}} = \frac{S^*(\omega) e^{i\omega T}}{\delta\pi R K} \delta(z - z_s).$$

This equation clearly shows the vertical focusing performed by the PCA at the range corresponding to the source location. It is worth mentioning that this vertical focusing is due to the closure property of the modes. If the array has only a few elements and cannot properly sample the propagating modes, one can conclude that this focusing will be degraded. As will be shown in this thesis, numerical simulations indicate that even with a small array aperture, a good quality of focus can be achieved.

### C. TIME REVERSAL ACOUSTICS IN A STATIC RANGE-DEPENDENT UNDERWATER ACOUSTIC CHANNEL

Consider a general range-dependent environment such that small regions in the vicinity of the source and in the vicinity of the vertical array are assumed to be range

independent, but the larger region between is allowed to have arbitrary range dependence in bathymetry and sound speed. In the ideal case, the vertical array spans the entire water column with elements having uniform spacing  $d$  and the modal eigenfunctions have negligible amplitude in the bottom. Ignoring absorption losses, the TRA field in the vicinity of the source is given by (Kuperman et al., 1998)

$$P_{TRA}(r', z, \omega) = S^*(\omega) e^{i\omega T} \sum_m \frac{\Psi_m(R, z) \Psi_m(R, z_s)}{8\pi\rho(z_s) K_m(0) d \sqrt{Rr'}} e^{iK_m(R)(r'-R)}, \quad (2.20)$$

where  $K_m(0)$  and  $K_m(R)$  are the modal eigenvalues evaluated at the vertical array and at the source, respectively.  $\Psi_m(R, z)$  represent the modal eigenfunctions at the array and  $d$  is the vertical array inter-element spacing.

In a situation that is not too far from this ideal case, Eq.(2.20) can be used to illustrate the properties that an actual array may possess. In this ideal case, the first property that one can notice from Eq.(2.20) is the independence of the focus field with respect to the range-dependent environment between the focus and the array. The focus depends only on the local properties of the water column and the sea floor, but it is not affected by bathymetry or range-dependent water column properties in the region between the array and the focus. Therefore Eq.(2.20) shows that, neglecting absorption losses and the cylindrical spreading factor  $\frac{1}{\sqrt{Rr'}}$ , the focus pattern is independent of the distance

between the source and the array. Thus all the general features of time-reversal acoustics discussed in this thesis should also exist in more general, range-dependent environments.

Losses due to absorption and scattering are expected to cause attenuation of higher-order modes. As a consequence, the focus becomes more blurry than that in the previous ideal lossless situation. Furthermore, as the distance between the array and the focus increases, the focus becomes blurrier due to the strong range and mode number dependence of attenuation. However, such influences will not be specifically treated in this analysis.



### **III. NUMERICAL MODELING OF THE TIME-REVERSAL ARRAY**

This chapter presents an overview of the parabolic equation (PE) model used for acoustic propagation modeling, as well as the method used for its implementation - the split-step Fourier (SSF) method (Hardin and Tappert, 1973). The Monterey-Miami Parabolic Equation (MMPE) model (Smith, 1996) is the acoustic propagation model used throughout this thesis. This propagation model is an upgraded version of the University of Miami Parabolic Equation (UMPE) model (Smith and Tappert, 1994). It is based on a parabolic equation approximation to the wave equation which was first introduced to the underwater acoustics community by Tappert (1974). This approximation is valid for lower frequencies (down to 2Hz) than the geometrical acoustic (small wavelength) approximation as it retains all the diffraction effects associated with the ocean sound channel (Tappert, 1977).

Other propagation methods such as the separation of variables are based on the approximation that the ocean is exactly horizontally stratified. In contrast, the parabolic equation model retains full coupling between local waveguide modes, making it valid for more realistic, non-stratified oceans. One of the main advantages of the PE/SSF implementation is the speed with which the acoustic field can be computed. These are some of the reasons why the use of parabolic approximation methods has become commonplace in the prediction of underwater acoustic propagation.

#### **A. PARABOLIC EQUATION THEORY**

The majority of the ocean environment is well suited for a description in cylindrical coordinates, particularly in the case of shallow water propagation where the range is much

larger than the ocean depth. For this reason, a cylindrical coordinate system is favored over others.

A time-harmonic acoustic field can be described in cylindrical coordinates by

$$P(r, z, \phi, t) = p_f(r, z, \phi) e^{-i2\pi f t}, \quad (3.1)$$

where  $p_f(r, z, \phi)$  is the frequency-dependent pressure amplitude as a function of radial range  $r$ , depth  $z$  (positive downward), and azimuthal bearing  $\phi$ . Substituting  $P(r, z, \phi, t)$  into the inhomogeneous wave equation with a point source leads to the Helmholtz equation in cylindrical coordinates (Jensen et al., 1994)

$$\frac{1}{r} \frac{\partial}{\partial r} \left( r \frac{\partial p_f}{\partial r} \right) + \frac{1}{r^2} \frac{\partial^2 p_f}{\partial \phi^2} + \frac{\partial^2 p_f}{\partial z^2} + k_o^2 n^2(r, z, \phi) p_f = -4\pi P_o \delta(\vec{r} - \vec{r}_s), \quad (3.2)$$

where  $n(r, z, \phi) = \frac{c_o}{c(r, z, \phi)}$  is the acoustic index of refraction,  $c_o$  is the reference sound speed,  $c(r, z, \phi)$  is the acoustic sound speed, and  $k_o = \frac{\omega}{c_o}$  is the reference wavenumber.

The right-hand term represents a point source at location  $\vec{r}_s = (r_s, z_s) = (0, z_s)$ , with pressure amplitude  $P_o$  defined at a reference distance  $|\vec{r} - \vec{r}_s| = 1m$ . Note that  $c(r, z, \phi)$  includes all the features of the environment, although density variations were neglected in this derivation. These density variations could be incorporated into a new index of refraction without any loss of generality.

Assuming the ocean acts as a waveguide, acoustic energy primarily propagates outward from the source in the horizontal direction. Therefore, the pressure field can be approximated by

$$p_f(r, z, \phi) = \psi_f(r, z, \phi) H_0^{(1)}(k_o r), \quad (3.3)$$

where  $\psi_f(r, z, \phi)$  is a slowly varying amplitude function that modulates the outgoing zero-th order Hankel function of the first kind,  $H_0^{(1)}(k_o r)$ . Using the far-field asymptotic expansion of the Hankel function (Gradshteyn and Ryzhik, 1994), the pressure field Eq.(3.3), may be defined by

$$p_f(r, z, \phi) = P_o \sqrt{\frac{R_o}{r}} \psi_f(r, z, \phi) e^{ik_o r}. \quad (3.4)$$

This equation provides the relationship between the acoustic amplitude  $p_f(r, z, \phi)$  and the so-called “*PE field function*”  $\psi_f(r, z, \phi)$ . The PE field function is normalized such that at  $r = R_o$ ,  $|\psi_f| = 1$  and  $|p_f| = P_o$ . Neglecting the cylindrical spreading  $\sqrt{\frac{R_o}{r}}$  factor and the range-dependent factor  $e^{ik_o r}$ , the PE field function  $\psi_f(r, z, \phi)$  can be considered as being the ocean transfer function at location  $(r, z, \phi)$  due to a source at location  $(r_s, z_s, \phi_s)$ .

Substituting Eq.(3.4) into the Helmholtz equation and separating the equations for the incoming and outgoing fields (e.g., Smith and Tappert, 1994), one can show that the defining equation for the PE field function is

$$\frac{i}{k_o} \frac{\partial}{\partial r} \psi_f(r, z, \phi) = (1 - Q_{op}) \psi_f(r, z, \phi), \quad (3.5)$$

where  $Q_{op}$  is the so-called “square-root operator” defined by



$$Q_{op} = \left[ \frac{i}{k_o} \frac{\partial^2}{\partial z^2} + (n^2 - 1) + 1 \right]^{\frac{1}{2}}. \quad (3.6)$$

Tappert (1977) introduced several approximations to  $Q_{op}$  including the standard parabolic equation (SPE). One of the key features of the SPE approximation is the separation of the operator  $Q_{op}$  into two independent operators,  $T_{op}$  and  $U_{op}$ , separating the depth derivative and environmental term, respectively. The equation defining the evolution of the field function  $\psi_f(r, z, \phi)$  then takes the form

$$\frac{i}{k_o} \frac{\partial}{\partial r} \psi_f(r, z, \phi) = \left( T_{op} \left( \frac{\partial^2}{\partial z^2} \right) + U_{op}(n) \right) \psi_f(r, z, \phi). \quad (3.7)$$

Thomson and Chapman (1983) introduced a higher order approximation based on an operator splitting by Feit and Fleck (1978), valid for higher angles of propagation and commonly known as the “wide-angle” (WAPE) approximation. In this approximation,

$$T_{op} = -\frac{1}{k_o^2} \frac{\partial^2}{\partial z^2} \left[ \left( 1 + \frac{1}{k_o^2} \frac{\partial^2}{\partial z^2} \right) + 1 \right]^{-1} \quad (3.8)$$

and

$$U_{op} = -(n - 1). \quad (3.9)$$

Jensen et al. (1994) suggests that this approximation extends the accuracy of the solutions to a half-bandwidth of  $40^\circ$  but benchmark testing using the WAPE approximation demonstrated the capability to accurately propagate fields for select environments with half-beamwidths greater than  $70^\circ$  (Chin-Bing et al., 1993). The WAPE approximation also features less sensitivity to the choice of  $c_o$  (reference sound speed), and the effects of

phase errors are greatly reduced in typical deep ocean conditions relative to the SPE approximation (Jensen et al., 1994 and Chin-Bing et al., 1993). For these reasons the WAPE approximation is the one used in the MMPE propagation model.

## B. PARABOLIC EQUATION NUMERICAL SOLUTION

In order to numerically solve the parabolic equation, the MMPE uses a split-step Fourier (SSF) algorithm (Hardin and Tappert, 1973). This is a marching algorithm that integrates the solution in range by applying the operator  $U_{op}$  in the  $z$ -domain and the operator  $T_{op}$  in the  $k_z$ -domain. The latter operator is defined in the  $k_z$ -domain (vertical wavenumber domain) as

$$\hat{T}_{op}(k_z) = 1 - \sqrt{1 - \frac{k_z^2}{k_o^2}}. \quad (3.10)$$

Note that both operators are just scalar multipliers and may be applied independently.

The approximate solution for  $\psi_f(r, z)$  is iterated in range from  $r$  to  $r + \Delta r$  according to (Smith and Tappert, 1994)

$$\psi_f(r + \Delta r, z) = e^{-ik_k \Delta r U_{op}(r, z)} \mathbf{F} \left( e^{-ik_o \Delta r \hat{T}_{op}(r, k_z)} [\mathbf{F}^{-1}(\psi_f(r, z))] \right), \quad (3.11)$$

where  $\mathbf{F}$  and  $\mathbf{F}^{-1}$  represent forward and inverse Fourier transformations, respectively. Note that Eq.(3.11) provides time-harmonic solutions to the PE field when substituted into Eqs. (3.4) and (3.1). Broadband results are obtained by solving Eq.(3.11) for an evenly-spaced discrete set of frequencies in the bandwidth of interest. For each time-harmonic solution, the output of the model is in the form of the complex PE field functions for each frequency

and spatial grid point,  $\psi_f(r_i, z_j)$ , referenced to a unit magnitude at  $r = 1\text{m}$ , and computed at the spatial grid points  $(r_i, z_j)$ .

### C. MONTEREY-MIAMI PARABOLIC EQUATION MODELING

The MMPE acoustic propagation model allows user-specification of the most important environmental parameters as inputs. In the model, the environment is divided into three distinct layers: the water column, the sediment layer and a deep bottom layer. In the water column the user can specify the range-dependent sound speed profile. For the sediment layer, the water/sediment bathymetry and several range-dependent acoustical parameters can be specified: the sound speed, the sound speed gradient, the density, compressional attenuation, shear speed and shear attenuation. All these parameters are depth-independent with the exception of the sound speed that has the specified gradient. For the deep bottom layer, the user must specify the same parameters as in the sediment layer. For a single bottom composition, the deep layer can be defined at a depth below the maximum computational depth thereby removing its influence from the calculation.

The MMPE model allows the use of two types of sources. A wide-angle source which approximates a point source and a vertical line array where steering is allowed. Source parameters that need to be specified are the depth, the center frequency, the bandwidth, and the number of discrete frequencies (should be a power of two for efficient FFT computation). The principal input data file specifies the name of the environmental data files, the name of the output binary file and other parameters such as the computational grid size, the computational range and depth, the output range of values and its grid size, and the reference sound speed. The output binary file consists of the PE field function evaluated on the output grid at the discrete set of frequencies. It includes a header with the

necessary environmental information for the post-processing of the PE field function. For more information about the contents of the environmental data files and for the source code in Fortran, the reader is referred to the Ocean Acoustics Library supported by the U.S. Office of Naval Research through the web page <http://oalib.njit.edu/pe.html>. From this web page the reader may also download the UMPE model documentation (Smith and Tappert, 1994).

#### D. TIME ARRIVAL STRUCTURE

It is assumed that the source transmits a single pulse  $s(t)$  centered at frequency  $f_o$  with a spectral shape  $S(f)$  over bandwidth  $BW$ . Note that the bandwidth  $BW$  corresponds to the bandwidth over which the acoustic field solutions need to be evaluated. The output of the MMPE model is the PE field function  $\psi_f(r, z)$  evaluated at  $N$  discrete frequencies in the bandwidth of interest, from  $f_c - \Delta f \frac{N}{2}$  to  $f_c + \Delta f \frac{(N-1)}{2}$ , where  $f_c$  is the carrier frequency and the frequency spacing  $\Delta f$  is given by  $\Delta f = \frac{BW}{N-1}$ . Due to the Fourier transform convention assumed, the time arrival structure at some distance  $r$  from the source requires the Fourier transformation of the pressure field  $p_f(r, z)$ . From Eq.(3.4), the pressure field is related to the PE field function by

$$p_f(r, z) = P_o \sqrt{\frac{R_o}{r}} \psi_f(r, z) e^{ik_o r}. \quad (3.12)$$

Taking into account the transmitted pulse spectrum, the corresponding pressure field becomes

$$p_f(r, z) = P_o \sqrt{\frac{R_o}{r}} \psi_f(r, z) S(f) e^{ik_o r}. \quad (3.13)$$

The arrival time structure of the propagating field may then be computed from

$$p(r, z, t) = P_o \sqrt{\frac{R_o}{r}} \int_{-\infty}^{\infty} \psi_f(r, z) S(f) e^{ik_o r} e^{-i2\pi f t} df. \quad (3.14)$$

Noting that we may write  $e^{ik_o r} = e^{i2\pi f \frac{r}{c_o}}$ , the result of this phase factor in Eq.(3.14) produces arrival time results in terms of "reduced time"

$$T = t - \frac{r}{c_o}, \quad (3.15)$$

where  $t$  is the absolute travel time of the pulse. Then

$$p(r, z, T) = P_o \sqrt{\frac{R_o}{r}} \int_{-\infty}^{\infty} \psi_f(r, z) S(f) e^{-i2\pi f T} df. \quad (3.16)$$

Finally, to decrease the computational burden associated with large transform sizes in evaluating the full Fourier transform, the MMPE model heterodynes the signal, downshifting the center frequency to d.c., and integrates only over the bandwidth such that

$$\tilde{p}(r, z, t) = P_o \sqrt{\frac{R_o}{r}} \int_{-\frac{BW}{2}}^{\frac{BW}{2}} \psi_{f+f_c}(r, z) S(f' + f_c) e^{-i2\pi f' T} df', \quad (3.17)$$

where  $f' = f - f_c$  and  $\tilde{p}(r, z, t)$  is the envelope of the pressure field. This will introduce a phase factor of  $e^{-i2\pi f_c T}$  in the time domain which can easily be added later.

At this point it is worth mentioning that  $N$ , the number of discrete frequencies and also the transform size, should be a power of two in order to use computationally-efficient FFT algorithms. Since the signal bandwidth is  $BW$  and the transform size is  $N$ , then

$$\Delta T = T_{k+1} - T_k = \frac{1}{BW}, \quad (3.18)$$

giving a time window of duration

$$T_{window} = (N-1) \cdot \Delta T = \frac{N-1}{BW}. \quad (3.19)$$

This time duration value turns out to be very important as a pulse propagates in the ocean and “stretches” in time due to multipath propagation. Therefore according to the bandwidth, the number of frequencies  $N$  should be chosen judiciously in order to avoid the undesired “wrap-around” effect due to pulse elongation greater than the time window. In practice, the minimum value for  $N$  is  $N = 2^L$ , where  $L = \lceil \log_2(BW) \rceil + 1$  and the delimiters invoke rounding up to the next integer.

## E. TIME DOMAIN ANIMATION OF SPATIAL ACOUSTIC PROPAGATION

For a better understanding of the mechanics of time reversal acoustics, it is very useful to look at time-domain snapshots of the acoustic field. In order to perform this analysis, the “reduced time” at each range  $r_i$  is converted to absolute time  $t_{ik} = T_k + \frac{r_i}{c_o}$ , converting  $p(r_i, z_j, T_k)$  to  $p(r_i, z_j, t_{ik})$ . The acoustic field can now be considered as being evaluated on a time-space grid defined by  $(r_i, z_j, t_{ik})$  where  $t_{ik}$  represents absolute time. Time-domain snapshots are then obtained by defining a specific “time-frame” such that  $t_{ik}=t_o$  and then evaluating  $p(r_i, z_j, t_o)$  at the ranges and depths of interest. Note that since

the width of the window  $T_{window}$  is finite, the total range extent  $R$  covered at any specific time is  $R=c_o T_{window}$

To obtain a "time-frame" in the range of interest, some constraints are required on the bandwidth of the signal  $BW$  and the range step of the output  $\Delta r$ . In general, the time difference between two grid points in range is

$$t_{(i+1)k} - t_{ik} = \frac{r_{i+1} - r_i}{c_o} = \frac{\Delta r}{c_o}. \quad (3.20)$$

The condition for a constant time-frame over different range points is

$$t_{(i+1)k} = t_{i(k+m)}. \quad (3.21)$$

Therefore, Eq.(3.20) becomes

$$t_{i(k+m)} - t_{ik} = m \cdot \Delta t = \frac{\Delta r}{c_o}. \quad (3.22)$$

For a given time resolution  $\Delta t$ , one can then have

$$\Delta r = mc_o \Delta t = m \frac{c_o}{BW}, \text{ with } m=1, 2, 3, \dots \quad (3.23)$$

where  $c_o$  is the reference sound speed and  $m$  is an integer different from zero. From Eq.(3.23), for a given  $BW$ , the maximum range resolution allowed in a time-frame is

$\Delta r = \frac{c_o}{BW}$ . For graphical reasons, a  $\Delta r$  that provides about 100 points in the range of

interest gives good results.

#### IV. ENVIRONMENTAL INFLUENCES IN TIME-REVERSAL ACOUSTICS

This chapter presents the results of PC array numerical simulations using the MMPE acoustic propagation model. Section 4.A gives a brief description of the UWA channel used throughout this chapter and Section 4.B gives the description of the transmitted signal envelope. Section 4.C gives a description of PC array focusing in the environment previously described and how the TRA technique is similar to matched field processing. Section 4.D presents a study of the effects that different carrier frequencies have on the focus properties. Section 4.E presents the frequency characterization of the channel transfer function in order to evaluate the possibility of bandwidth degradation in the channel. In Sections 4.F and 4.G several PC array configurations are considered. Section 4.F shows the effects of changing the element spacing and Section 4.G shows the effects of changing the PC array length (or array aperture). Section 4.H presents an implementation of focus range shifting. Depending on the source depth, the focus will change its location in range when the PC array changes the carrier frequency of the transmitted signals.

During the TRA examination process that lead to this thesis several other environments were considered. In all these environments it was observed that the PCA has similar focusing properties as the ones described for the UWA channel considered in this chapter. For conciseness, only the environment described in Section 4.A will be examined here because it is the most realistic of the cases considered. The other UWA channels that were considered include channels with different sound speed structures and different range-independent as well as range-dependent bathymetry.



## A. ENVIRONMENT CHARACTERIZATION

The UWA environment used throughout this chapter to study the properties of PC arrays is presented in Figure 4.1. This UWA channel is range-independent because the sound speed profile, bottom bathymetry and bottom characteristics do not change along the range. As depicted in Figure 4.1, the source is located at a range of 0m and a depth of

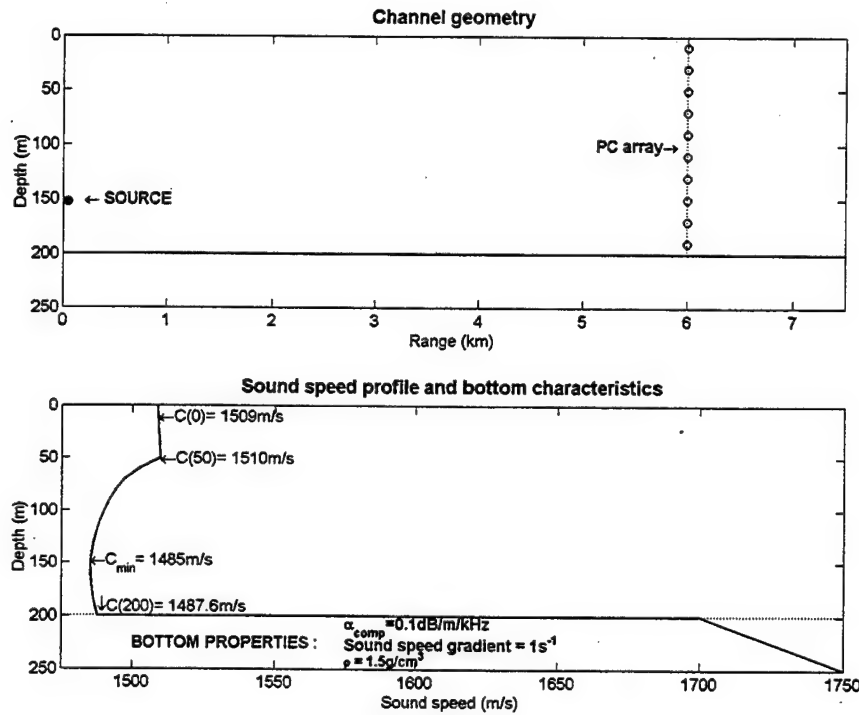


Figure 4.1. UWA Channel Profile.

150m, and the vertical PC array is located 6km from the source. The PC array in Figure 4.1 represents an illustration of its location with respect to the source. Throughout this chapter several array configurations will be used. In some cases the PC array may have different element spacing, in other cases it has different lengths and in some cases it can span the entire water column.

Figure 4.1 also shows the sound speed profile and the bottom characteristics. This environment has an upward refracting sound speed profile from a depth of 0m to 50m. From 50m to the bottom at 200m, this UWA channel exhibits a sound speed profile similar to a typical shallow ocean sound speed structure with the sound axis (minimum value of the sound speed) located at 150m in depth. The bottom has compressional attenuation of 0.1dB/m/kHz, a sound speed gradient of  $1\text{s}^{-1}$  and a density of  $1.5\text{g/cm}^3$ .

## **B. TRANSMITTED SIGNAL ENVELOPE**

In most of the TRA numerical simulations presented in this chapter, the transmitted pulse has a carrier frequency of 800Hz. The exceptions are in Section 4.D where carrier frequencies of 400Hz and 1200Hz are used. In each case, the transmitted pulse has a bandwidth of 100Hz with a -3dB effective bandwidth of 36.6Hz. The MMPE computational bandwidth over which the solutions of the PE field functions are computed includes the full 100Hz. The envelope characterization of the transmitted pulse is given in Figure 4.2. It should be mentioned that the spectrum of the transmitted pulse envelope is given by the coefficients of a Hanning window (Proakis and Manolakis, 1996). Therefore the lower panel in Figure 4.2 represents a Hanning window (in dB units) that spans 100Hz in frequency. The time domain representation of the corresponding signal at a carrier frequency of 800Hz can be found in the third panel of Figure 1.2 on page 6. For this signal, the -3dB pulse width is 14.1ms.

## **C. TIME REVERSAL ACOUSTICS IN A RANGE-INDEPENDENT ENVIRONMENT**

For the environment described in Section 4.A, Figure 4.3 represents the magnitude of the ocean response for a time-harmonic acoustic source at a frequency of 800Hz in a vertical plane defined by the source and the array elements. The ocean frequency response

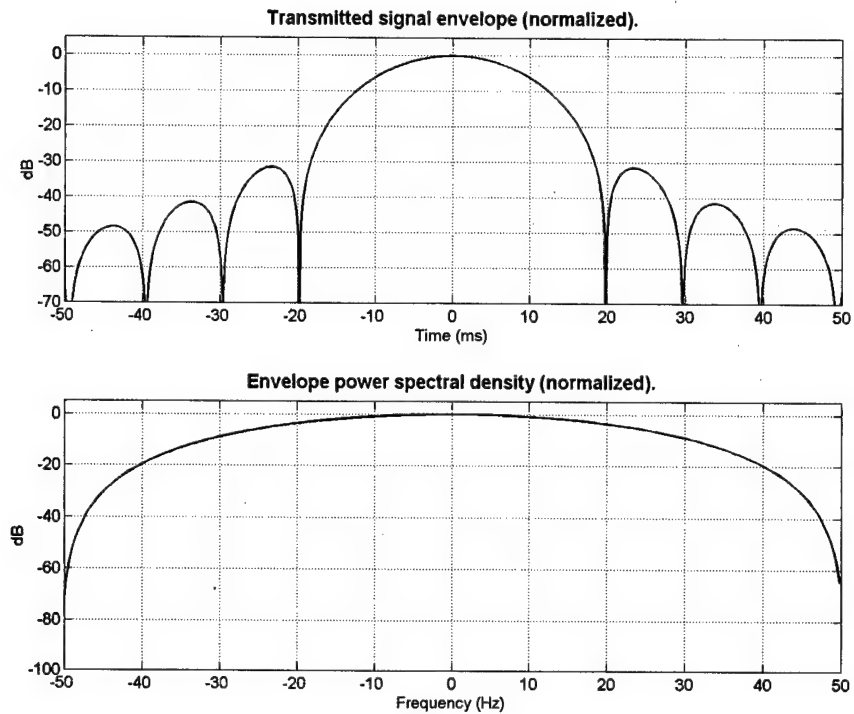


Figure 4.2. Transmitted Signal Envelope.

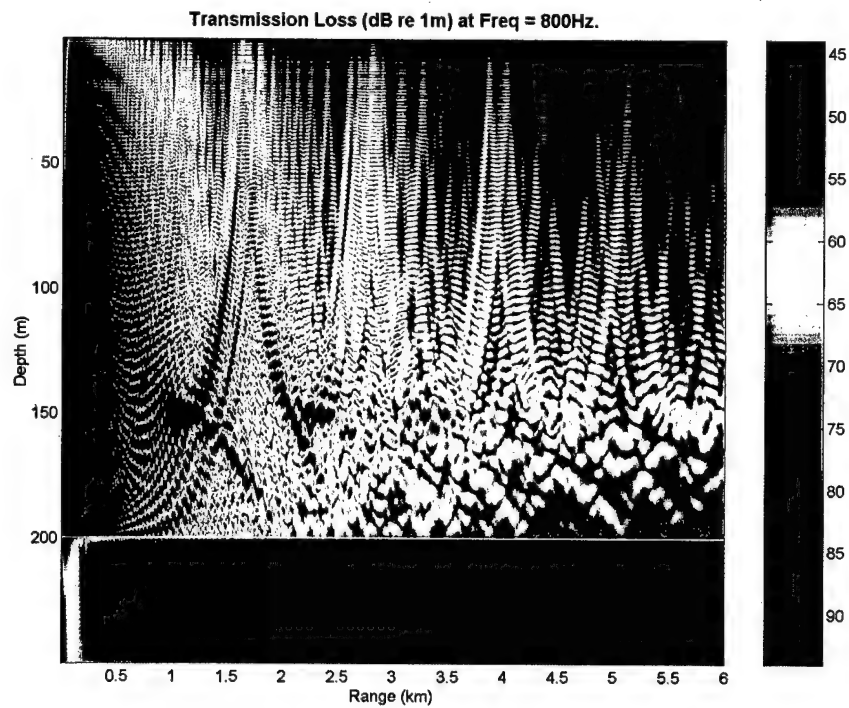


Figure 4.3. Ocean Response at 800Hz.

at 800Hz is represented in terms of transmission loss (dB re 1m). Considering the ocean as a spatial filter, Figure 4.3 represents the “forward propagation transfer function” at the frequency of 800Hz. The term “forward propagation” is used to denote the propagation from the acoustic source. If the source located at a depth of 150m transmits a pulse at the carrier frequency of 800Hz with a bandwidth of 100Hz (-3dB effective bandwidth of 36.6Hz), the time arrival structure at the vertical array may be evaluated by Fourier synthesis of single frequency (CW) solutions over the bandwidth of interest. The time and frequency domain characterization of the transmitted pulse was previously described in Figure 4.2.

Figure 4.4 represents the time arrival structure of the received signal envelope at the PCA for the 800Hz signal with 100Hz bandwidth. For a given array element, the envelope of the received signal is given by the corresponding horizontal line at the array element

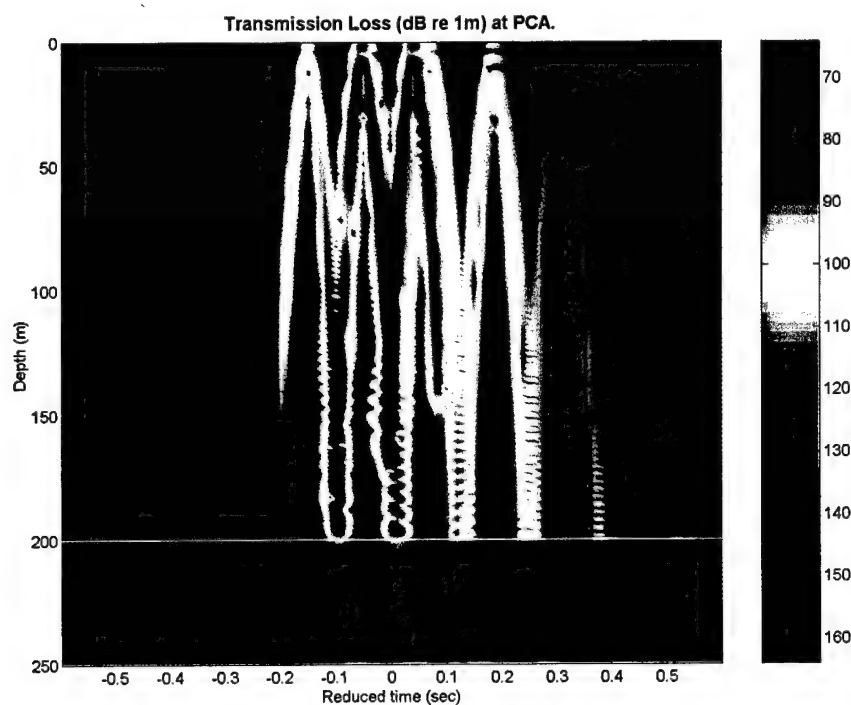


Figure 4.4. Time Arrival Structure at the PCA.

depth. The effects of multipath propagation are clearly observed in Figure 4.4 where any array element detects several multipath arrivals. From Figure 4.4 one can see that the multipath structure is similar between closely spaced array elements. The diversity between array elements can be exhibited by computing the envelope cross-correlation of the time arrival structure represented in Figure 4.4. The envelope cross-correlation shown in Figure 4.5 was computed with respect to the envelope received by the array element at a depth of 150m. With respect to this array element one can observe that the other array

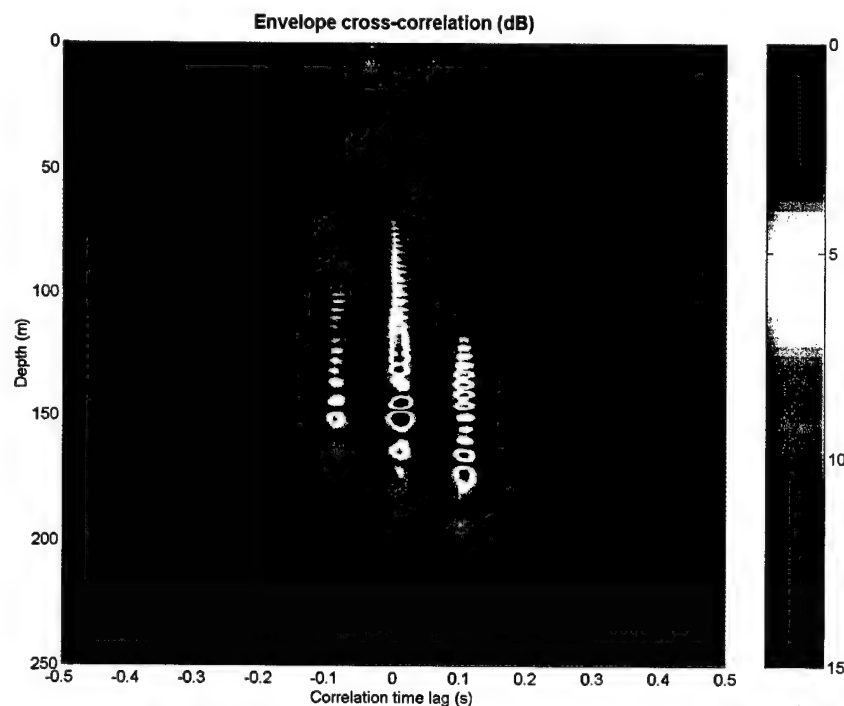


Figure 4.5. Envelope Cross-Correlation across the Array Elements.

elements become more decorrelated as the depth difference between array elements increases. In general as the distance between array elements increases the multipath structure becomes more decorrelated. This spatial decorrelation between array elements is due to the presence of multipaths and is used in communication systems that explore the spatial diversity in the water column.

At the PCA, the received signals are time-reversed and transmitted back to the source. Figure 4.6 represents the ocean frequency response to the time-reversed acoustic field transmitted by the PCA evaluated at 800Hz. At this point it should be mentioned that the

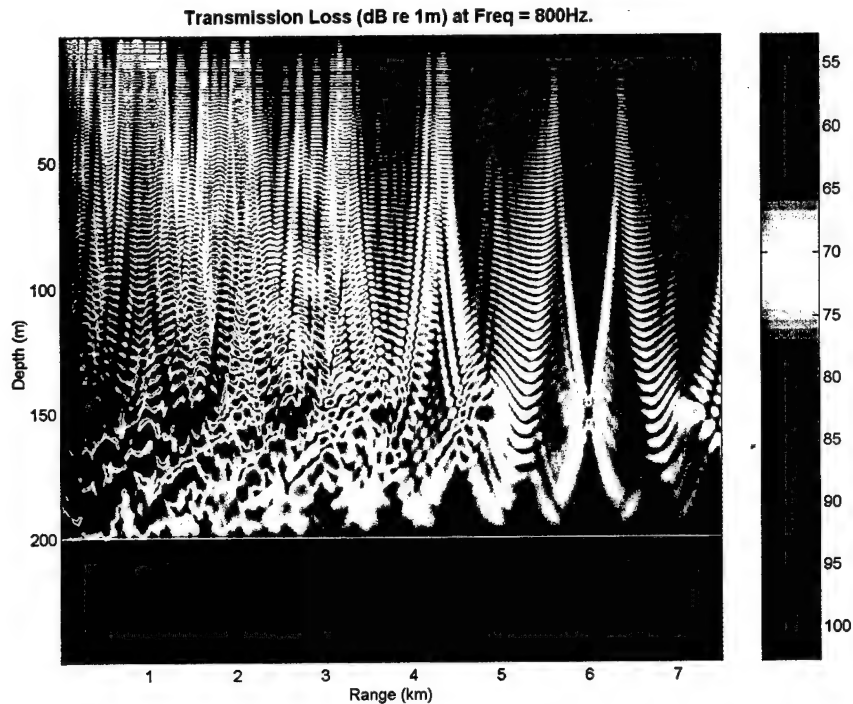


Figure 4.6. Backward Propagation Ocean Response at 800Hz.

term “backward propagation” will be used throughout this thesis and by that is meant propagation of the time-reversed signals from the PCA through the reciprocal environment. From this perspective, Figure 4.6 represents the back propagation ocean frequency response at 800Hz.

In Figure 4.6, the propagation is from the left to the right, i.e. the PCA is located at range 0km and spans the entire water column. In this geometry the original source is located at a range of 6km and at a depth of 150m. As expected, the phase conjugation of the 800Hz frequency component and its consequent propagation through the channel produces a strong spatial focus at the source location.

From the viewpoint of linear systems theory, the ocean itself behaves similarly to a spatial matched filter. Due to spatial reciprocity, the only location in space where this spatial filter is matched to the forward propagation function is at the source location. Therefore the output of this spatial filter is maximized at the source location creating a strong focusing effect because the source location is the spatial location where the backward propagation transfer function matches the forward propagation transfer function. In other words, at the source location all multipath contributions will arrive in phase and add constructively creating the focusing effect. Using these same arguments, all the other frequency components of the transmitted pulse will focus at the source location. Figure 4.7 represents the time arrival structure of the back propagated pulse ( $f_c=800\text{Hz}$ ,  $BW=100\text{Hz}$ ) at the source range and the temporal, vertical and horizontal PCA focusing properties. The data displayed corresponds to the recorded signals of a vertical array of elements that spans the entire water column at the source range.

In Figure 4.7 one can observe the temporal focusing at the source location where the multipath structure is greatly suppressed. This temporal focusing is also a consequence of the matched filter behavior of the ocean where all frequency components will arrive at the same time at the same location. In this numerical simulation the PCA spans the entire water column with an element spacing of  $d = 0.244\text{m}$  and  $\lambda/d = 7.67$ , approaching the ideal case of a continuous line of sources. As a consequence, the temporal sidelobes represent the limiting situation that can be achieved in practice. As will be shown in this chapter, decreasing the number of array elements increases the temporal sidelobes.

Also note in Figure 4.7 that this focusing process has vertical (along the depth) sidelobes. As mentioned in Chapter II, the vertical focusing is a consequence of the

closure property of the propagating modes. Thus, these sidelobes appear in part because there are higher order modes, called evanescent modes (Jensen et al., 1994), that decay rapidly in range and don't propagate in the channel. In addition, some propagating modes

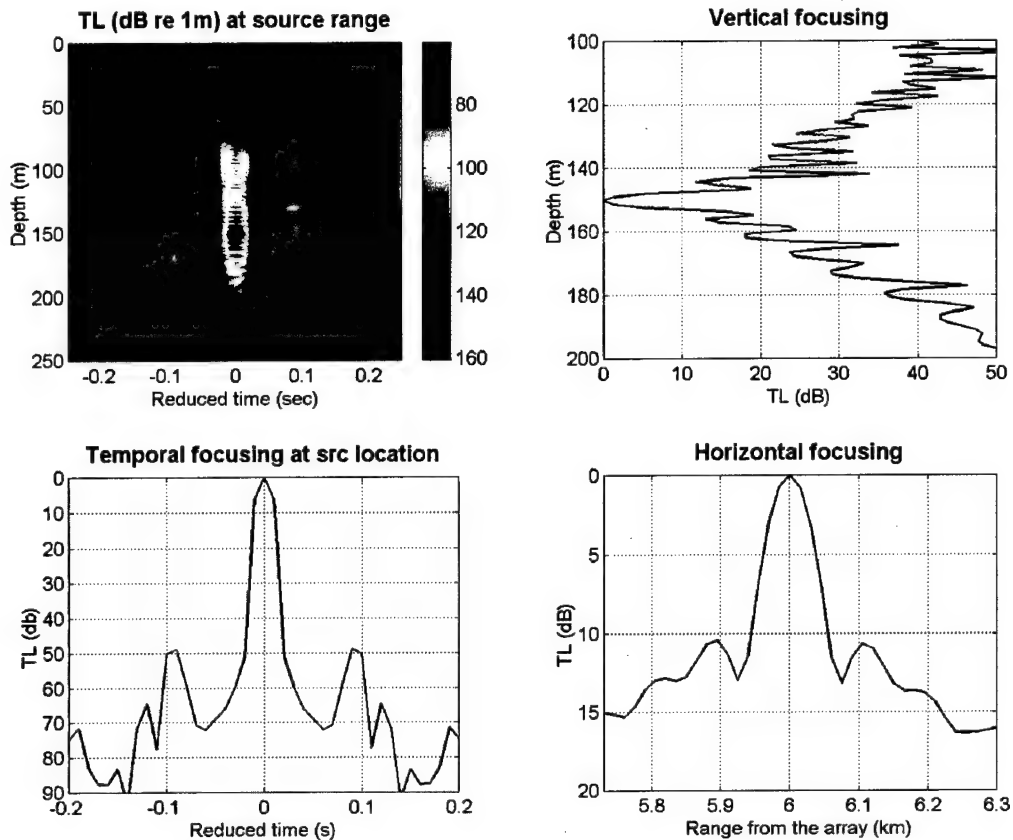


Figure 4.7. Time Arrival Structure Focus Range. Temporal, Vertical and Horizontal PCA Focusing Properties.

are attenuated differently by the environment. Thus the focusing extent is dependent on the number of modes allowed in the channel.

Also displayed in Figure 4.7 is the horizontal focusing at the source depth. This plot is very representative because it gives the maximum amplitude of the received signal envelope for a given location in range. The main lobe is located at 6km corresponding to the source range and the -3dB main lobe width is about 60m, much larger than the corresponding value along the depth which is 3.3m.



#### D. FOCUSING AT DIFFERENT FREQUENCIES

In this case study, three signals with carrier frequencies of 400Hz, 800Hz and 1200Hz were used. All these signals have the same bandwidth of 100Hz that corresponds to a -3dB effective bandwidth of 36.6Hz, the same envelope spectral shape as described by Figure 4.2 and the PC array spans the entire water column. The temporal, vertical, and horizontal focusing properties for each signal are displayed in Figure 4.8.

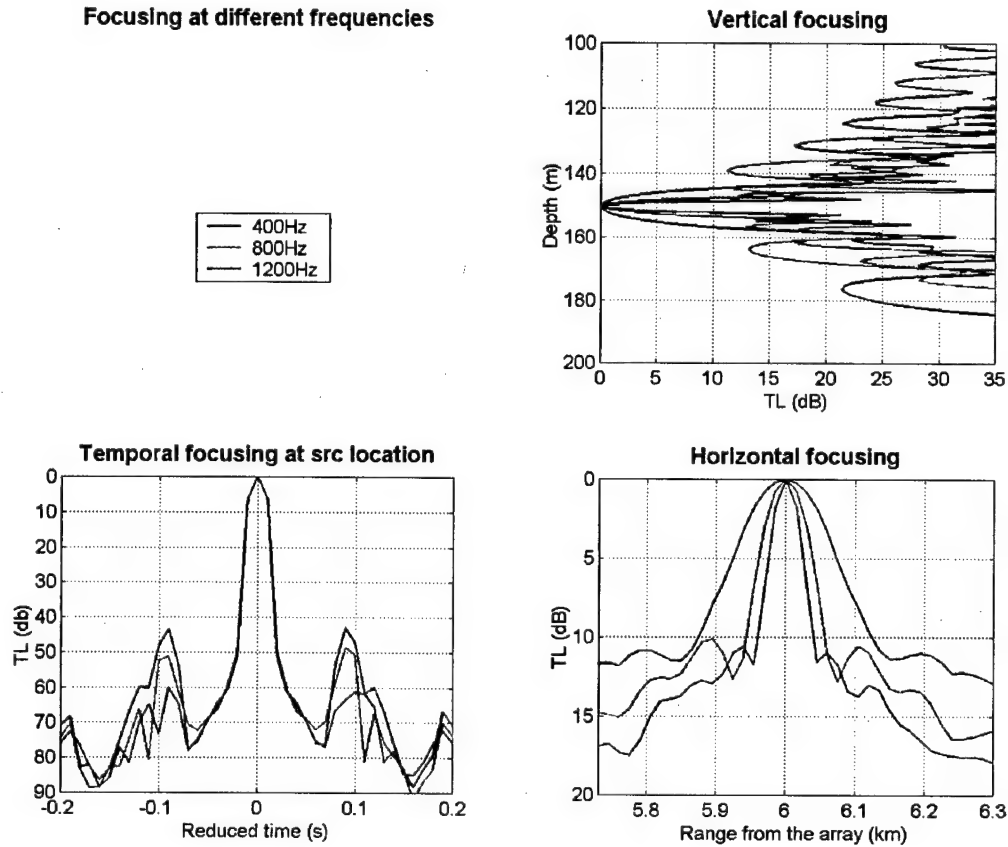


Figure 4.8. Focusing at Different Frequencies.

As shown in Figure 4.8 the temporal duration of the main arrival is identical for any of these test cases. This is a significant result because it means that using the same bandwidth at different carrier frequencies achieves the same temporal pulse resolution and consequently the same symbol rates. It appears that the channel frequency response does

not change significantly over the bandwidth of each signal and therefore the same temporal resolution exists at these different carrier frequencies. The temporal sidelobes are below 40dB and decrease with increasing frequency. This is presumably due to the increase in the number of propagating modes at higher frequencies. In addition, the focus dimensions (or "footprint") are found to decrease with increasing frequency. This is due to a combination of the increase in the number of propagating modes and the decrease in acoustic wavelength.

### E. CHANNEL CHARACTERIZATION IN THE FREQUENCY DOMAIN

For the channel described in Figure 4.1 where the source is 150m deep and the PC array spans the entire water column, Figure 4.9 represents the forward propagation channel frequency response evaluated at the PC array element 150m deep. The upper

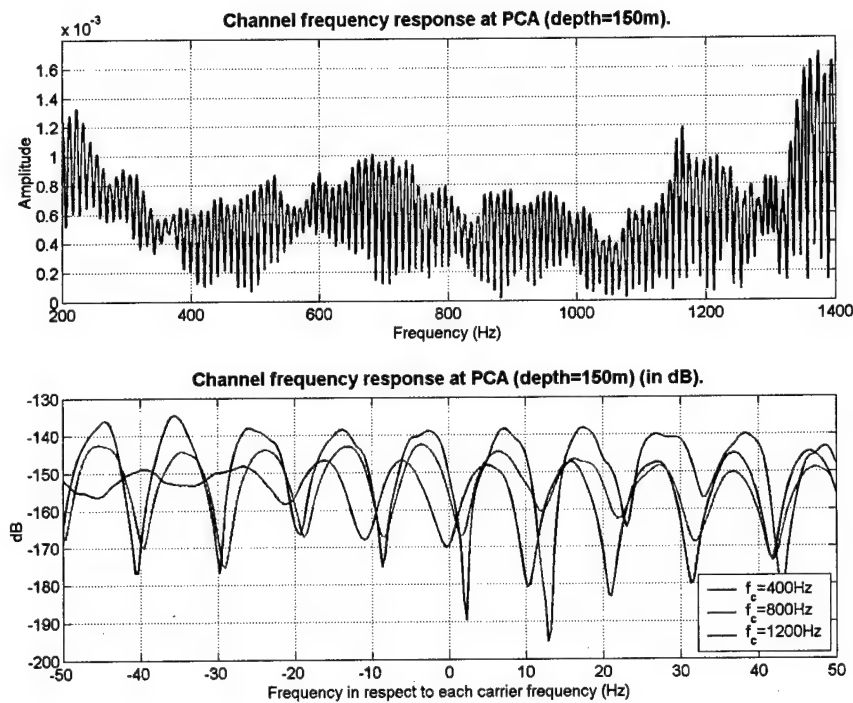


Figure 4.9. Forward Propagation Channel Frequency Response at the PC Array Element Located 150m Deep.

panel represents the frequency response from 200Hz to 1400Hz and the lower panel represents the channel frequency response in the range of frequencies used in the previous section. Regarding the lower panel one can observe that the channel frequency response has smooth peaks and deep fades almost evenly spaced. In some cases the deep fades can be 50dB below the peak level. This behavior in the forward propagation frequency response is a consequence of the multipath interference structure at this array element. For the other PC array elements the channel frequency response exhibits similar behavior with the deep fades located at different frequencies that the ones shown in this example.

Figure 4.10 represents the channel frequency response at the focus location. This channel frequency response will be designated by “two-way” frequency response because it includes forward propagation followed by backward propagation to the focus location. Comparing Figure 4.9 with Figure 4.10, the two-way propagation frequency response

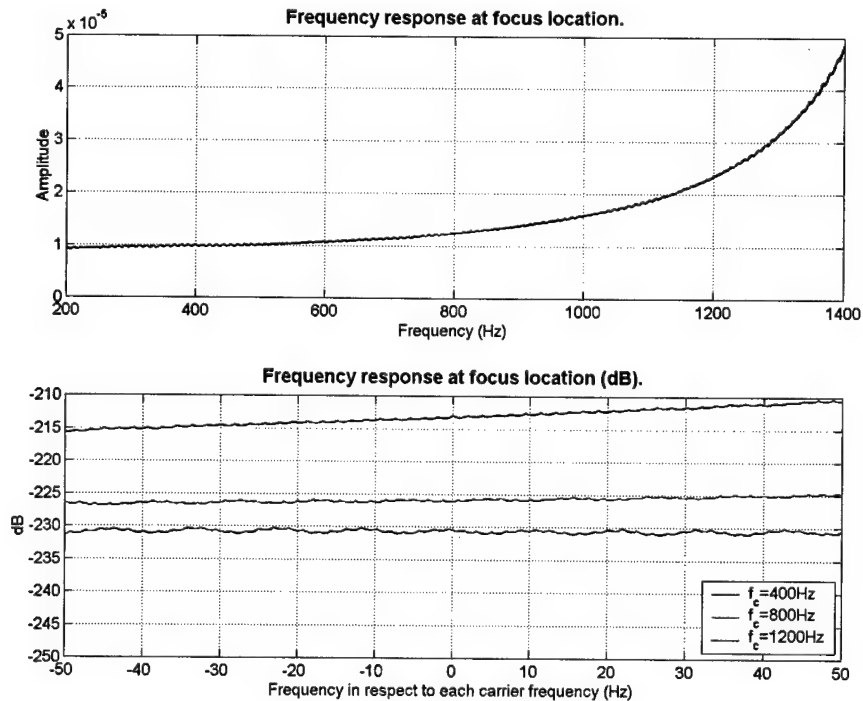


Figure 4.10. TwoWay Channel Frequency Response at Focus Location.

evaluated at the focus location exhibits a smooth behavior with frequency where the deep fades are absent indicating that all frequency components at the focus location are in phase. Note however that the lower frequency components at the focus have lower amplitude than higher frequency components. This is presumably due to stronger interaction of the low frequency modes with the lossy bottom.

In Figure 4.9, only the frequency response for the 150m deep array element is shown. Since the PC array spans the entire water column and the interference structure will change along the depth, the other PC array elements will exhibit nulls in the frequency response at frequencies other than the ones shown for this PCA element. When back propagation is performed, the contributions from all the PC array elements will add coherently at the focus location, restoring all frequency components in the received field. Thus, at the focus location the two-way frequency response is much smoother than for the forward propagation case.

#### **F. EFFECT OF INTER-ELEMENT SPACING**

In this section we evaluate the influence on the focus due to PC arrays with different element spacing. In this test case the transmitted signal has a carrier frequency of 800Hz and a bandwidth of 100Hz. The geometry of the different PC arrays used in this study is given in Figure 4.11 where each array is identified by a number from 1 to 6. Associated with each PCA are 3 numbers giving the number of elements, the distance between consecutive elements in meters and the distance between consecutive elements in terms of carrier wavelengths. Note that PCA number 1 has the smallest element spacing and that the distance between array elements doubles between consecutive arrays.

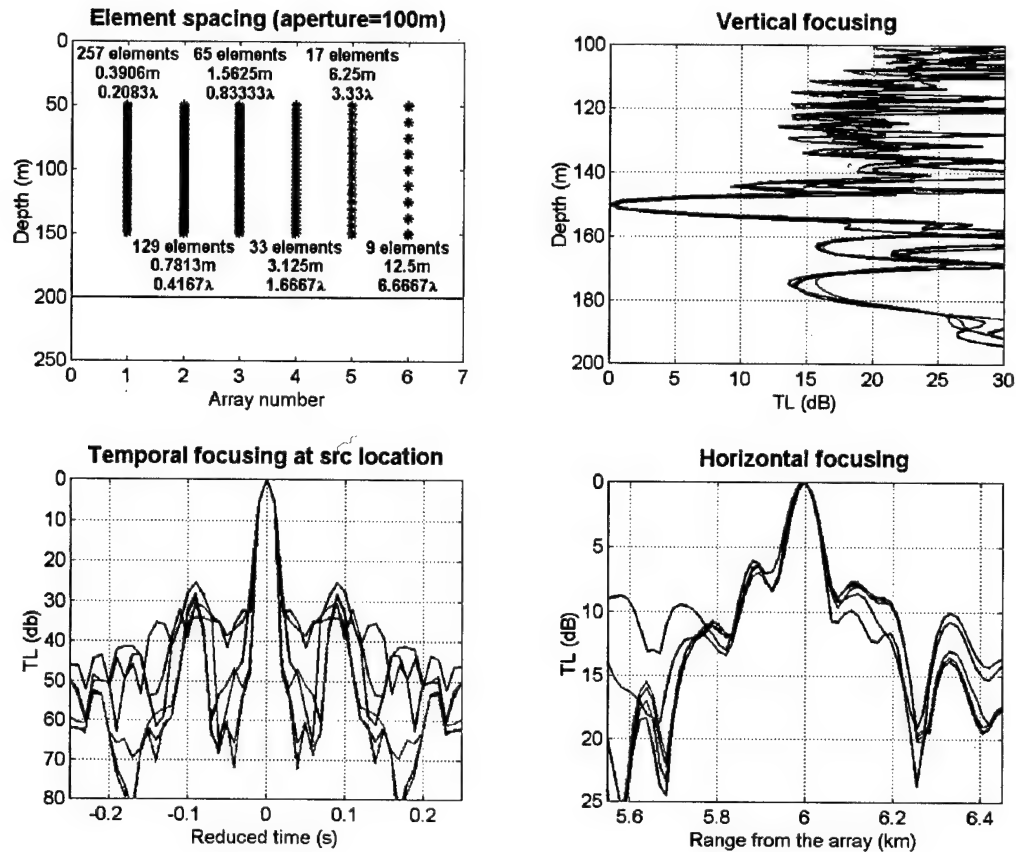


Figure 4.11. Focusing Properties Using PC Arrays with Different Element Spacing.

Starting from PCA number 1 to number 6, as the element spacing increases, the array cannot provide enough spatial sampling of higher-order propagating modes. Thus, the focusing degrades as a result of the lack of resolution of higher order modes in the field. From a linear systems point of view the changing in focus is the result of removing array elements that are more correlated, i.e. as the array spacing increases it increases the decorrelation between array elements.

From Figure 4.11 one can conclude that the spatial dimensions of the focus do not change significantly for these PCA configurations. Comparing these results to Figure 4.7 where the PCA spans the entire water column one should expect an increase in temporal

sidelobes because the PC arrays in Figure 4.11 only span half of the water column, collecting less information about the channel conditions. Remarkably, in the worst case situation (PCA number 6 with only 9 elements), the temporal sidelobes are 25dB below the main lobe. These results seem to indicate that even with a small number of array elements, a good focusing quality can be achieved provided that the PCA has enough spatial sampling of the propagating modes in the water column.

### **G. EFFECT OF APERTURE SIZE**

In this study the element spacing is kept constant in order to evaluate the effect that different PCA aperture sizes have on the focus quality. The geometry and spatial location in the water column of the different PC arrays is depicted in Figure 4.12. In this figure, each array is designated by a number from 1 to 5. The numbers associated to each array give the number of array elements and the array length in meters and in carrier wavelengths. As the PCA aperture size increases, it can provide a better sampling of the low-order propagating modes. Starting with array number 1 and going to array number 5, the changes in focus are due to better spatial sampling of the low-order propagating modes. Thus, one should expect better focusing properties as the aperture size increases because the PCA has more spatial diversity and provides a better sampling of the channel conditions.

Because these PCA arrays cannot properly sample low-order propagating modes, the sidelobes increase in the depth and range coordinates. In Figure 4.12 the first three arrays with apertures of  $2.5\lambda_c$ ,  $5\lambda_c$  and  $10\lambda_c$ , respectively, have temporal sidelobes about 12dB below the main lobe. When the aperture size increases to  $20\lambda_c$  and  $40\lambda_c$ , the temporal sidelobes decrease to 27dB and 35dB, respectively, below the main lobe. This distinctive

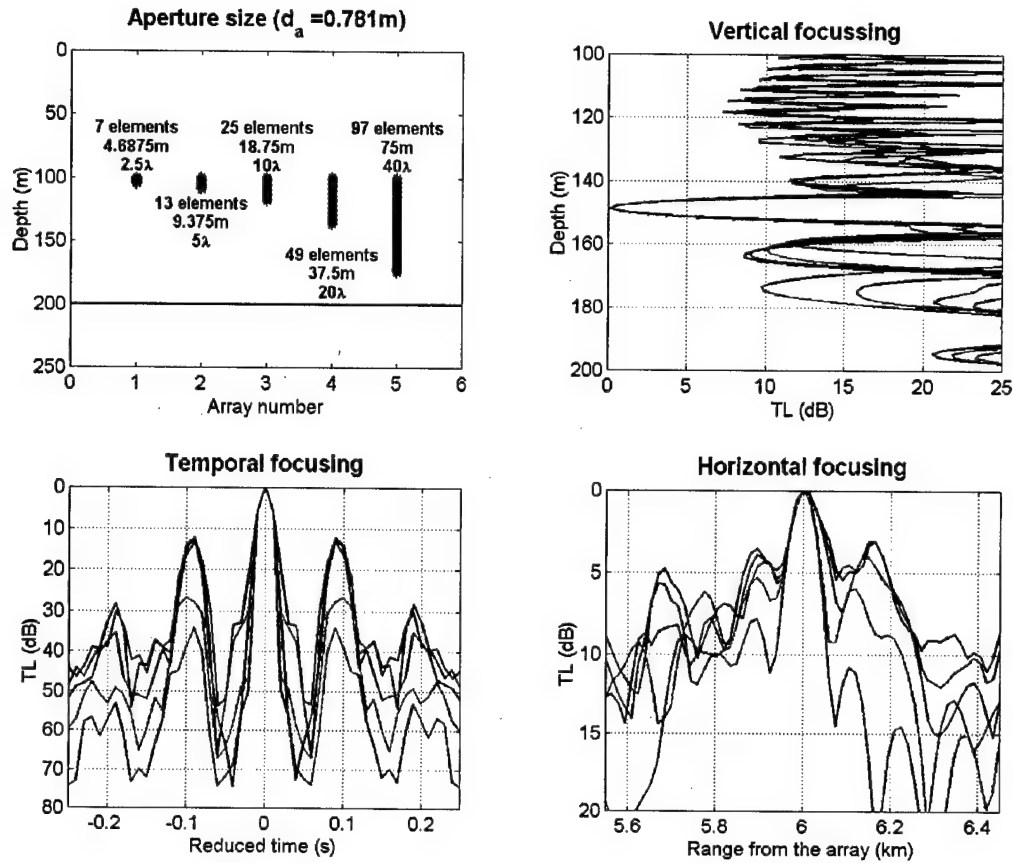


Figure 4.12. Focusing Properties Using PC Arrays with Different Aperture Size.

behavior of array numbers 4 and 5 compared to the other three is because they provide a better sampling of the lowest-order propagating modes and therefore have better temporal properties.

Presumably, the placement of these arrays in depth will also affect the focus quality. The best quality focus would be expected when the array is placed at a depth which optimally samples the dominant propagating modes. The conclusion that can be drawn is that in a given environment one should evaluate the most important propagating modes and use an array aperture that provides enough sampling of these modes.

## H. EFFECT OF FREQUENCY BIN SHIFTING ON FOCUSING AT OTHER LOCATIONS IN RANGE

The basic idea of the range shifting approach is that the PCA can focus at different ranges by increasing or decreasing the carrier frequency of the transmitted signal. This frequency shifting of the carrier frequency can be implemented in near real time by an FFT bin shift at the PCA array before transmission.

This procedure is based on the acoustic-field invariant property in the coordinates of frequency and range (Brekhovskikh and Lysanov, 1991). It has been shown (Chuprov and Mal'tsev, 1981, and Chuprov, 1982) that the interference structure in oceanic waveguides is characterized by the existence of lines of maximum intensity  $I(\omega, r)$  having a slope  $\beta$ , and this slope is an invariant for a particular group of modes (Song et al., 1998),

$$\beta = \frac{r}{\omega} \left( \frac{\Delta r}{\Delta \omega} \right) = \frac{d(1/v)}{d(1/u)} \quad (4.1)$$

where  $v$  and  $u$  are the phase and group velocities characterizing a given mode group, respectively. The invariant  $\beta$  is determined by the properties of the channel and the derivative in Eq.(4.1) averaged over this group.

This invariant property applies not only to the sound intensity but also to the phase velocity and envelope (group) delay (Grachev, 1993) thus extending to broadband pulse propagation. From Eq.(4.1), if the PCA transmits the complex conjugated field at a carrier frequency of  $\omega_c + \Delta \omega$ , the corresponding range shift is given by

$$\Delta r = \frac{1}{\beta} \frac{r_f}{\omega_c} \Delta \omega. \quad (4.2)$$



The results in Figure 4.13 show that range shifting was attained when the PCA receives a signal at a carrier frequency of 800Hz with 100Hz bandwidth and shifts the carrier frequency up or down by 2.5Hz and 5Hz. These results show that when the carrier

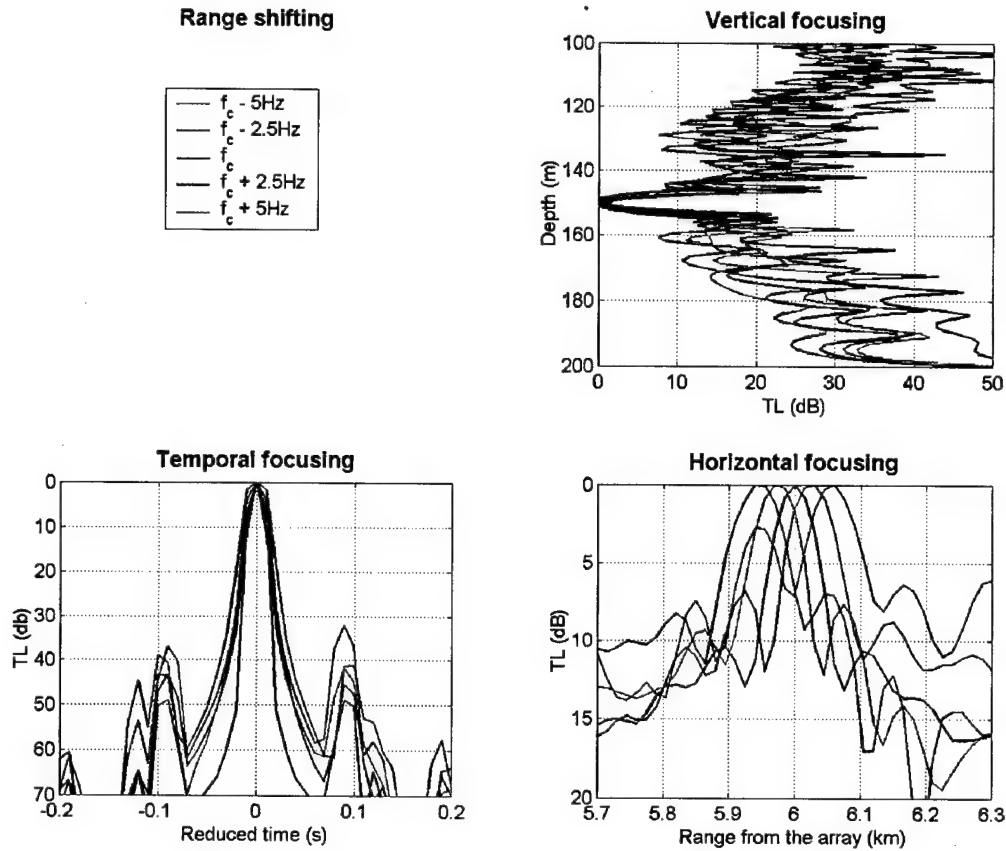


Figure 4.13. Focus Range Shifting by Changing the Carrier Frequency at PCA.

frequency is shifted by  $\pm 2.5\text{Hz}$ , the focus range shifts 30m with respect to the focus location at the nominal carrier frequency. When the carrier frequency is shifted by  $\pm 5\text{Hz}$ , the focus range changes by 60m. These results give an approximate value for the invariant  $\beta$  of 0.119. This range shifting property was also observed when the source was located 50m and 100m deep and by shifting the carrier frequency by  $\pm 2.5\text{Hz}$  and  $\pm 5\text{Hz}$ , giving a value for  $\beta$  of 0.228 and 0.258, respectively. The results in Figures 4.14 and 4.15

correspond to a source depth of 50m and 100m, respectively. At this point it seems clear that this invariant  $\beta$  has depth dependency.

It should be mentioned that the range shifting property can be observed as long as  $\Delta\omega$  is small when compared to the transmitted signal bandwidth. In other situations where  $\pm 20$  Hz and  $\pm 40$  Hz shifts were used, some dissimilar results were found. For these carrier shifts, no range shifting was observed when the source was located 150m deep. When the source was located 50m and 100m deep, it was observed that the focus split into two foci. These two foci are symmetrical in range with respect to the nominal focus range (no range shifting) and are also symmetrical in depth with respect to the nominal focus depth.

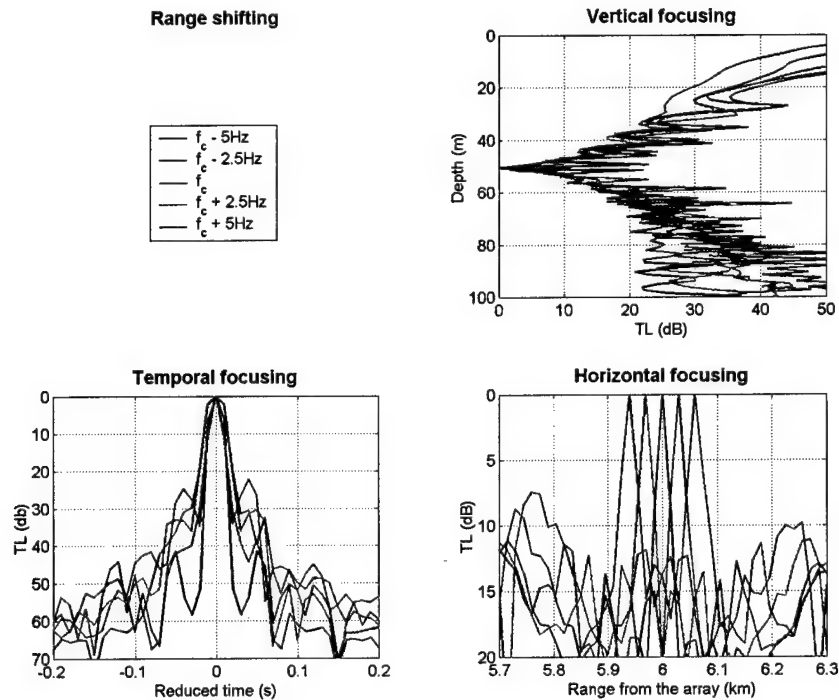


Figure 4.14. Focus Range Shifting for a Source 50m Deep.

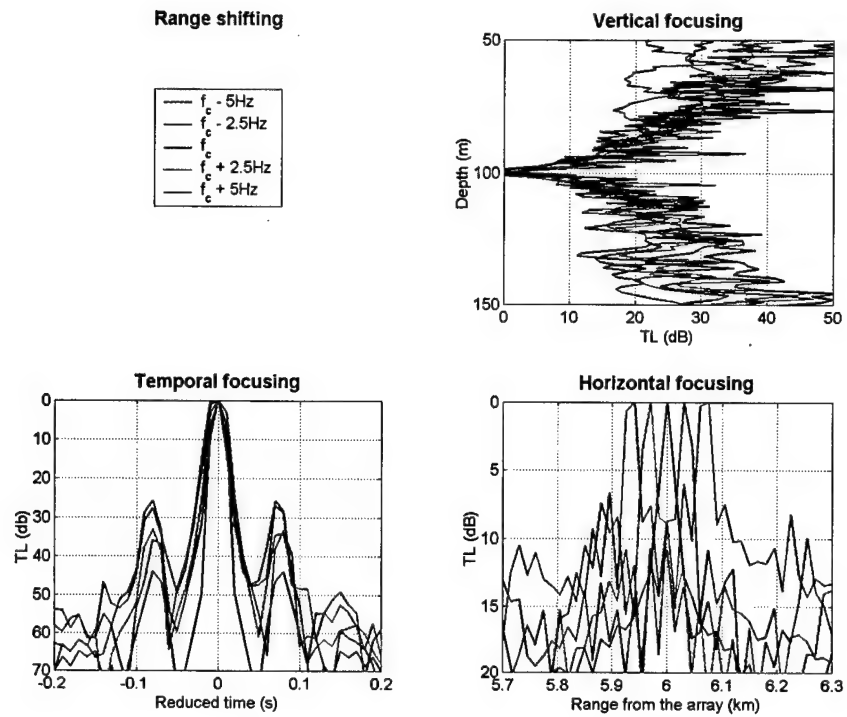


Figure 4.15. Focus Range Shifting for a Source 100m Deep.

## **V. APPLICATION OF TIME REVERSAL ACOUSTICS TO SHALLOW WATER COMMUNICATION SYSTEMS**

This chapter illustrates the application of TRA to UWA communication systems. It illustrates the use of PC arrays both in a point-to-point acoustic link and in a network situation. The communication system described in this chapter uses a reduced-complexity non-coherent detector at the expense of increased complexity in the transmitter (PCA). The examples illustrated in this chapter correspond to a nominal signaling rate of 30.5 symbols/second where 4 bits of information are encoded in each symbol, as described in Section 5.C. The channel used in this chapter for numerical simulations is the one described in Section 4.A.

### **A. USING PHASE-CONJUGATED ARRAYS IN UNDERWATER ACOUSTIC COMMUNICATIONS**

In this section, an example of the use of PC arrays in UWA communications is given. Figure 5.1 describes the simplest case of point-to-point communications between 2 stationary communication nodes. Each communications node of Figure 5.1 has a PC array that spans the entire water column and the source/receiver element of each node is located at a depth of 150m.

As seen in the previous chapter, when the time-reversed acoustic field propagates in the channel, it will focus back at the original source location due to spatial reciprocity. From the viewpoint of systems theory, the channel can be considered a spatial filter. In the forward propagation case (acoustic propagation from a source to a PCA), the presence of multipath and other channel distortions causes a different channel impulse response at different locations in the channel. After back propagation from each element of the PCA,

the channel behaves like a matched filter where the original source location is the only location in space where the forward propagation transfer function matches the backward propagation transfer function for each PC array element. Therefore during backpropagation the output of this spatial filter will be maximized at the source location. From these observations one can conclude that the source position is the optimal location in space to place a receiver.

For each node in Figure 5.1, the PCA focusing properties require the acoustic source to be co-located with the designated receiver element for TRA UWA communications. This receiver element will be responsible for reception of the TRA UWA communication signals. At this point is possible to conceive that each node will be using a single-element transducer that can be operated both as an acoustic source and as an acoustic receiver.

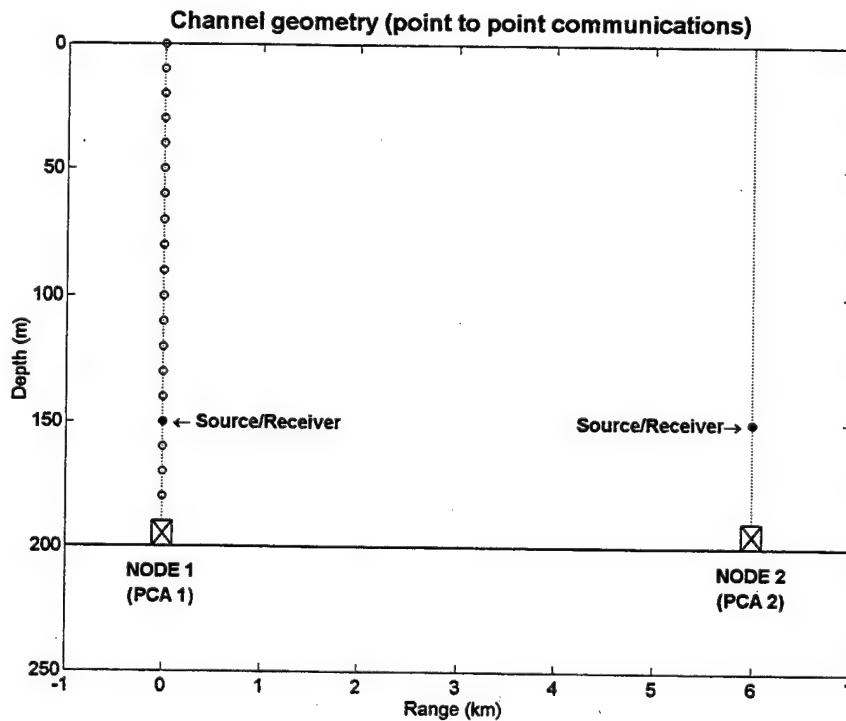


Figure 5.1. Channel Geometry in a Point to Point Communication Link.

The first step towards the focusing of PCA 1 requires a probe (pilot) pulse transmission from the node 2 acoustic source. As this probe pulse propagates, it will incorporate channel distortions including multipath. In the next step, the received acoustic signals at each PCA 1 element are digitized and stored in digital memories. For PCA 1 transmission (or backpropagation), the recorded signals will be time-reversed and transmitted by each PCA 1 element. The time-reversal transformation at PCA 1 is a simple task to perform, requiring the digital memories to be read in a last-in-first-out (LIFO) manner. At the PCA transmission, each element is excited by the output of the corresponding memory where the received signals were recorded.

In order to attain good focusing quality there is the requirement that all PCA elements must be synchronized at reception and transmission. By synchronization is meant that it will record the received signals during the same time interval and at transmission all the elements are fired at same time.

At this point one can consider that PCA 1 is "focused" at the source/receiver location of node 2 because it has recorded the necessary environmental information to generate a spatial focus at the node 2 source/receiver location. A similar process can be described for the focusing of PCA 2 that requires a probe pulse transmission from the node 1 acoustic source.

The PCA's focusing procedure is a critical aspect in a TRA communication link. TRA communications can only be established after both arrays are focused. In a real situation one must take into account the temporal variability of channel conditions. Focusing will degrade with time, requiring periodic PCA re-focusing. In a real situation where generally the nodes may have some motion, the PC array may need to update the environmental

information every time the receiver moves out of focus. In such a situation, the range shifting property of the PC array discussed in the previous chapter may be a very useful feature in a UWA communication system. If the receiver is moving slowly, the PCA is able to keep the focus at the receiver location, decreasing the rate at which the UWA communication system updates the environmental information (probing).

As a final remark the electronic circuitry associated with each PCA element includes a receiver amplifier, an A/D converter, digital filters, memory, a D/A converter and a transmitter amplifier. Until this point no reference was made to the presence of digital filters at each PCA array element. Its presence will become clear in the next section.

## **B. SIGNALING SCHEME**

In this section, a signaling scheme appropriate for PCA non-coherent communications is described. In this signaling scheme each symbol represents a 4-bit word giving a total of 16 different words in the code. Since this communication system is based on non-coherent detection, the value of each bit within a symbol is given by the detection or lack of detection of the corresponding frequency component. There are 15 different symbols in the code having at least one spectral component. The "all-zeros" word corresponds to the case where no carrier frequencies are detected. This signaling scheme corresponds to a QFSK modulation scheme. Thus, a simple receiver can be built based on a four element filter bank followed by an envelope detector. The detection of a given frequency component is achieved when the corresponding envelope detector output is higher than a given threshold.

In this signaling scheme, four frequency components are defined centered at 750Hz, 800Hz, 850Hz and 900Hz. Each one of these frequency components spans 100Hz in

frequency and has a -3dB bandwidth of 36.6Hz. The least significant bit corresponds to the frequency component centered at 900Hz and the most significant bit corresponds to the component at 750Hz.

To initialize the PC array, the source at each node must transmit each 100Hz bandwidth probe pulse separately. An alternative approach to simplify probe pulse transmissions would require that each PCA element has a bank of 4 digital filters centered at 750Hz, 800Hz, 850Hz and 900Hz. This way the array can store the frequency component contents from the arrival of a single probe pulse covering the entire bandwidth, 700Hz to 950Hz.

If the first approach is chosen there is no requirement for a digital filter bank in each PCA element but each node must make sure that the probe pulse transmissions will not overlap in time at the PCA.

The choice of which approach to use may be dictated by the temporal variability of the channel conditions that will degrade focusing, requiring periodic update of the channel conditions. The filter bank approach has the advantage that it requires only one probe pulse transmission from each source in Figure 5.1. Thus the communication system spends less time in array focusing and higher data throughput can be attained at the expense of a more complex PCA.

### **C. PHASE-CONJUGATED ARRAY**

In this section it is assumed that the PCA is able to learn the environmental information in the bandwidth of interest. The PCA is not in a shadow zone and each source transmits a probe pulse with bandwidth wide enough to accommodate the bandwidth used to transmit all individual frequency components of the signaling scheme.



The signaling scheme described in the previous section requires a four element filter bank for each PCA element. This four element filter bank frequency response is given in Figure 5.2. All the filters have the same spectral shape but different center frequency, each filter frequency response spanning over 100Hz giving a -3dB bandwidth of 36.6Hz. The frequency response of each filter is specified by the coefficients of a Hanning window. In Figure 5.2 the center frequency of each filter corresponds to the center frequency of one of the frequency components used in the signaling scheme.

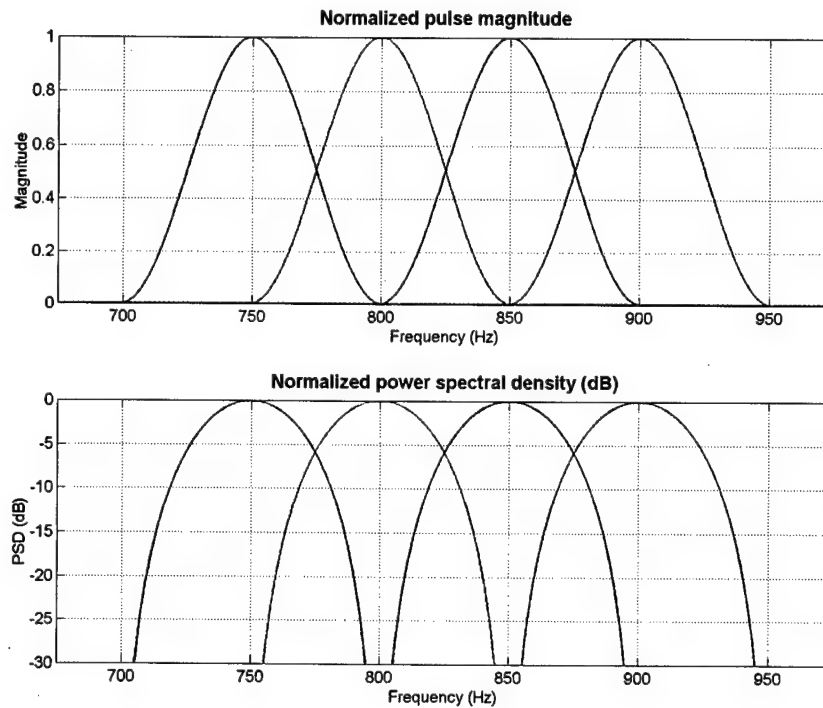


Figure 5.2. PCA Element Filter Bank Frequency Response.

After PCA reception and filtering, each PCA element will have recorded 4 different signals with different center frequencies. Each one of these signals will have the transfer function of the channel imprinted on it. As seen in the previous chapter, if all PCA elements transmit only the signal component centered at 800Hz, a pulse with 800Hz carrier frequency and a -3dB bandwidth of 36.6Hz will be received at focus location.

#### D. POINT TO POINT MESSAGE TRANSMISSION

This section presents a numerical simulation where a message is sent from node 1 to node 2 of Figure 5.1. At each PCA 1 element, the transmitted signal corresponding to a given symbol can be obtained by time-domain superposition (i.e., simultaneous transmission) of its different frequency components. Similarly the signal corresponding to a sequence of symbols can be obtained by superposition of the signals corresponding to the different symbols, properly delayed in the time domain. This time-domain delay corresponds to the signaling period and should be greater than the temporal duration of each symbol at the receiver location to avoid inter-symbol interference. In this case each symbol component will have at the receiver a -3dB temporal width of 14.1ms and a conservative value of 32.8ms was chosen for the signaling period. This provides a signaling rate of 30.5 symbols/second. This choice for the signaling period is somewhat arbitrary and based simply on producing results with clearly distinguishable arrivals. With accurate processing techniques, smaller signaling periods could be used thereby increasing the signaling rate.

Figure 5.3 presents the spectrogram of the signal corresponding to a message composed by the sequence of words from  $(0001)_b$  to  $(1111)_b$  that is intended to be transmitted from node 1 to the node 2 receiver. Figure 5.3 represents the ideal signal that node 1 wants to focus at the node 2 receiver. Note that the least significant bit corresponds to the frequency component centered at 900Hz and the most significant bit corresponds to the component at 750Hz.

Figure 5.4 presents the results from a numerical simulation where node 1 spans the entire water column and transmits the appropriate signals to focus the message of Figure

5.3 at the node 2 receiver. All the signals in Figure 5.4 are collected at a depth of 150m. The upper-left panel represents the signal transmitted from the PCA 1 element located at 150m depth while the other three correspond to the signal spectrogram at various ranges.

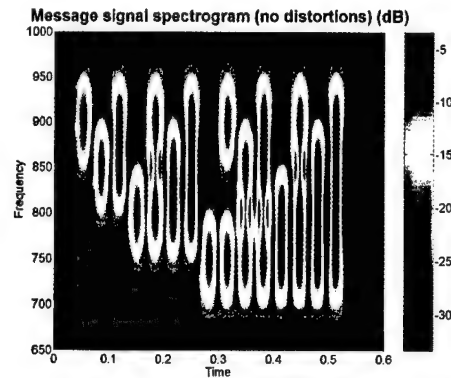


Figure 5.3. Spectrogram of the Signal Containing the Desired Message if no Distortions are Present in the Channel.

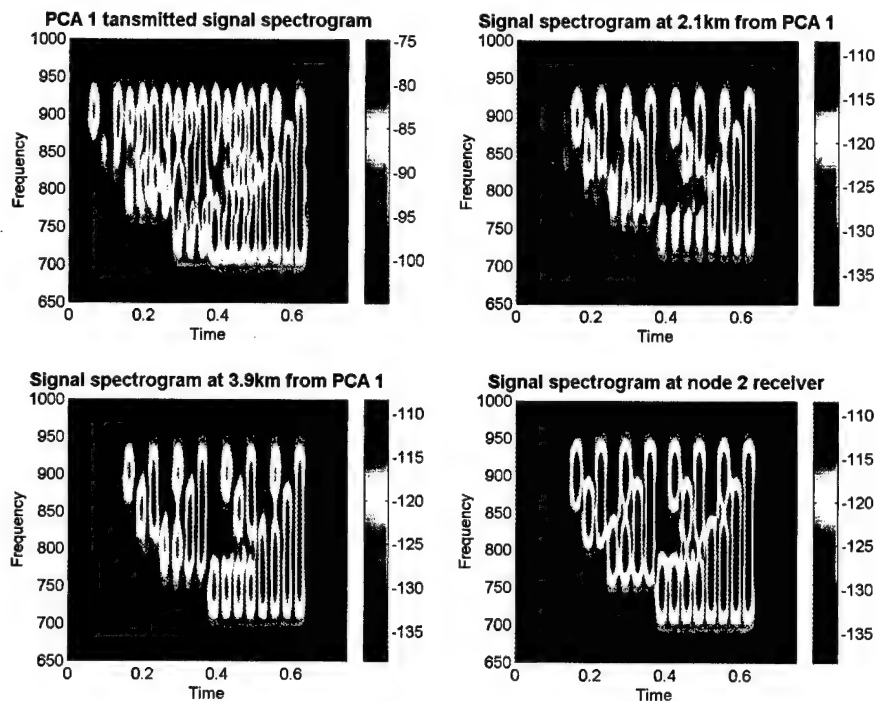


Figure 5.4. Message Signal Spectrogram Received by a Single Element Receiver 150m Deep, Evaluated at the PCA (Upper Left), at Two Intermediate Ranges and at the Focus (Lower Right).

Only the lower right panel in Figure. 5.4 corresponds to the signal spectrogram at the focus location.

In Figure 5.4 one can clearly observe that as the pulse back-propagates in the channel the multipath structure becomes less significant as the range approaches the focusing range. It can also be seen that when the pulse approaches the focusing range it increases the power spectral density of its spectral components. This increase in the power spectral density is a consequence of the vertical, horizontal and temporal PCA focusing properties as the sequence of symbols approaches the focus location.

#### E. PHASE-CONJUGATED ARRAY VERTICAL DIVERSITY IN UNDERWATER COMMUNICATIONS

Presented in this section is an extension of the TRA technique described in the previous sections. The setting for this TRA experiment is depicted in Figure 5.5 and is

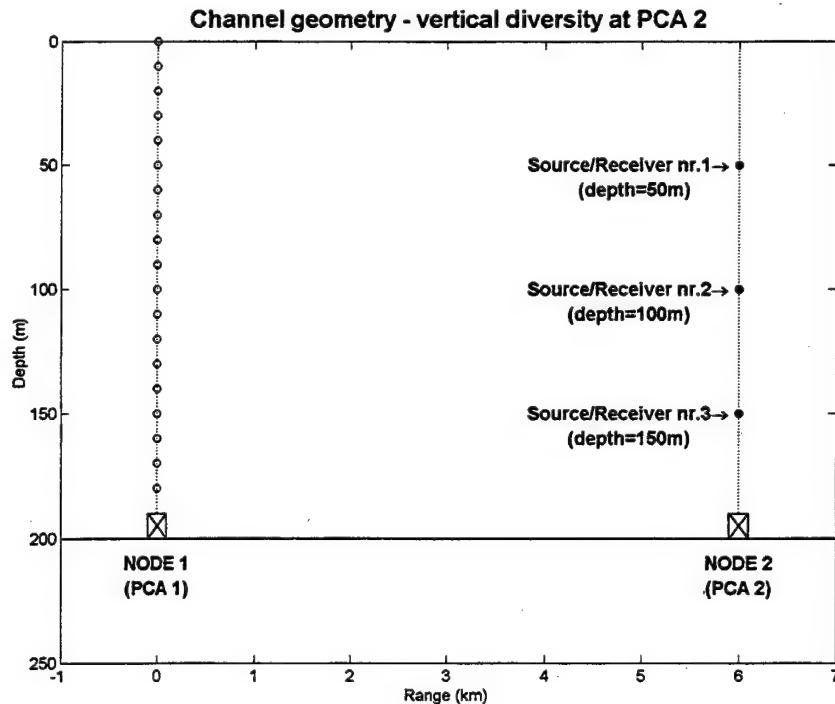


Figure 5.5. PCA Geometry for Vertical Diversity Examination.

similar to the one presented in Figure 5.1 with the difference that node 2 has now 3 source/receiver elements. The extension of the TRA technique presented in this section exploits node 1 PCA vertical diversity to focus the back propagated acoustic field at the different node 2 receiver locations. As a result, higher data throughputs can be achieved in the data link from node 1 to node 2 by simultaneously transmitting symbols designed to focus at different node 2 receivers.

In this case the PCA 1 focusing process requires probe pulse transmissions from each source/receiver element of node 2. The transmission of probe pulses from node 2 has the constraint that it must allow enough time between consecutive transmissions so each pulse will arrive at PCA 1 at different time slots and the pulses do not interfere. In this example PCA 1 will require a data bank with 3 times the storage capacity of the one used in PCA 2 because it has to store the signals received from 3 probe pulses. The TRA acoustic link from node 1 to node 2 can accommodate 3 times the data throughput of the case presented in the previous sections. In this case node 2 has 3 receivers and node 1 is able to send 3 different symbols (one for each node 2 receiver) during each symbol period.

At transmission, PCA 1 will assemble the message intended for each receiver by the superposition of its frequency components stored in its data bank. The signal transmitted by each PCA 1 element will be composed of the superposition of the signals for the different node 2 receivers. Figure 5.6 represents the desired message signal spectrogram that node 1 wants to focus at each node 2 receiver. Note that these signals do not correspond to the actual signals sent by PCA 1 elements. At each PCA 1 element the transmitted signal will include multipath and other channel distortions.

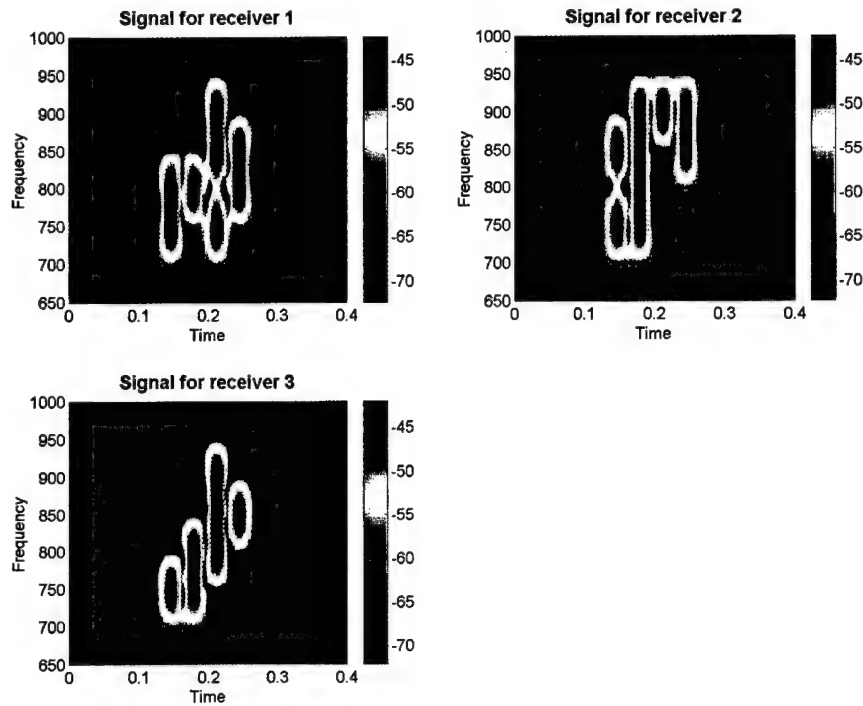


Figure 5.6. Desired Message Signals for Node 2 Receivers.

Figure 5.7 presents numerical simulation results of the PCA 1 transmitted signal propagation in which Figure 5.6 represents the message that PCA 1 wants to focus at each receiver location. In this simulation, PCA 1 spans the entire water column and the upper-left panel of Figure 5.7 represents the actual signal sent by the element located at a depth of 150m. We can observe multipath structure and strong interference between the different transmitted messages. The remaining panels in Figure 5.7 represent the signal received by each one of the node 2 receivers. Due to the vertical focusing properties of PCA 1, these results show very little message intersymbol interference at each receiver and the desired message can be easily decoded.

With respect to this same numerical simulation, Figure 5.8 represents the signal spectrogram at different ranges between node 1 and node 2 collected at a depth of 150m.

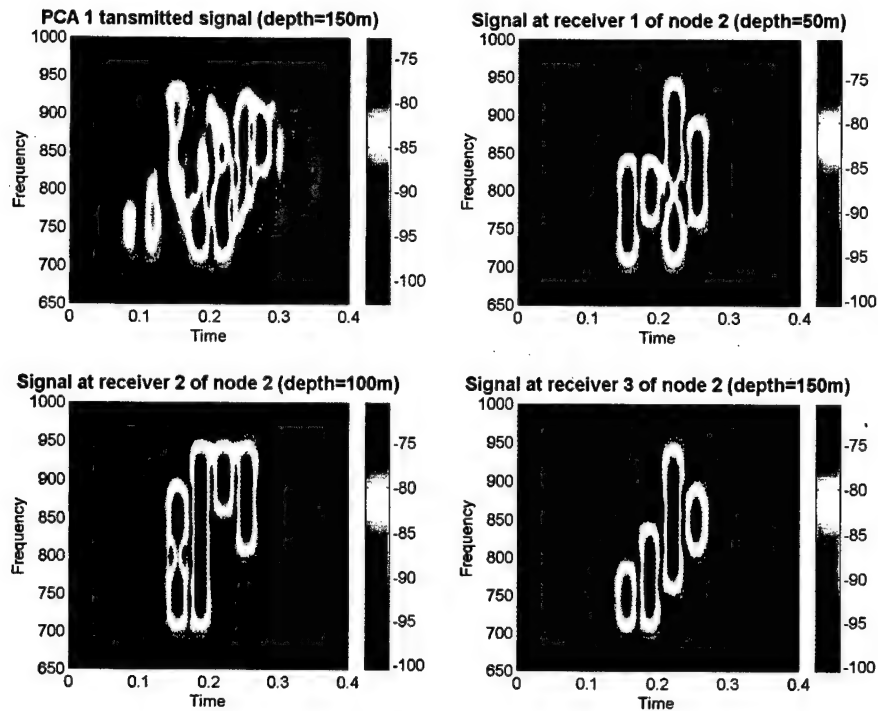


Figure 5.7. Transmitted Signal by PCA 1 and Received Signals at Node 2 Receivers.

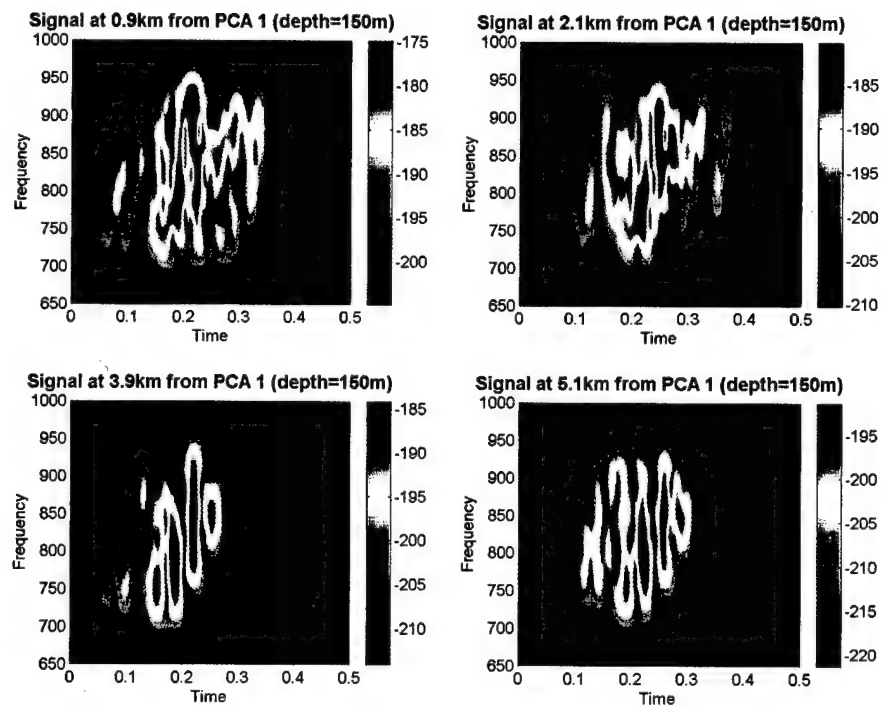


Figure 5.8. Received Signal Spectrogram at Depth of 150m and Different Ranges from PCA 1.

The results in this figure show that it will be extremely difficult to decode the original messages at these locations because the different message signals are overlapping both in time and in frequency. These results also show that this TRA vertical diversity technique may have applications to UWA secure communication links. Channel distortions and signal overlap both in time and frequency of the different messages seems to be a very good way to encode digital communication signals with the advantages of a higher data throughput.

#### F. PHASE-CONJUGATED ARRAY SPATIAL DIVERSITY IN UNDERWATER COMMUNICATIONS

In this section the concept described in the previous section is further extended to consider the case of an UWA communication network. The spatial arrangement of the acoustic network illustrated in this section can be observed in Figure 5.9. In this case all

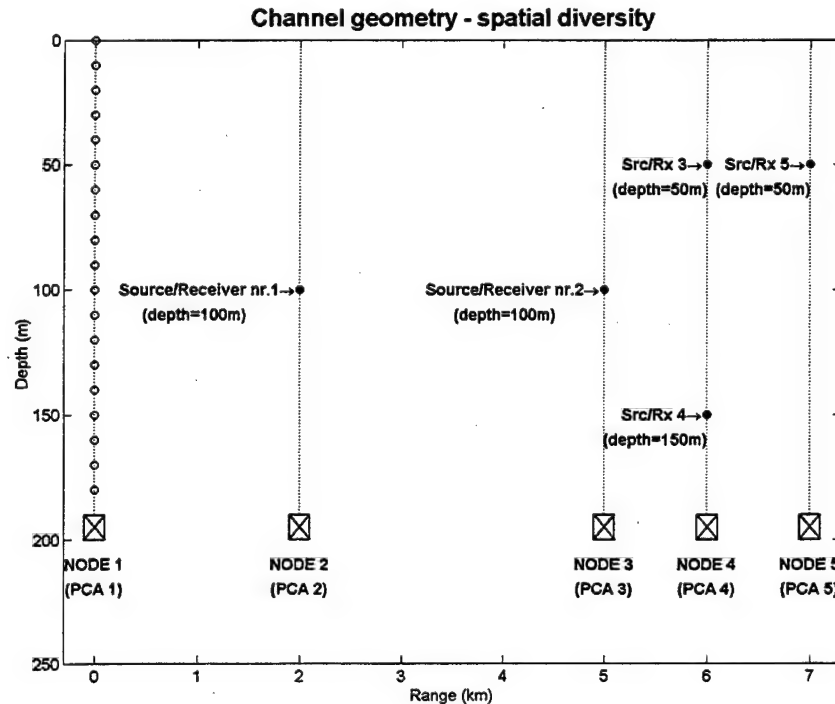


Figure 5.9. PCA 1 Geometry for Examination of Vertical and Horizontal Spatial Diversity in a UWA Communication Network.



the acoustic nodes are located in the same vertical plane. This constraint is only due to the fact that MMPE is a 2-dimensional propagation model, and therefore all the sources and receivers must be in the same vertical plane. In a real situation one could have these acoustic nodes located in different azimuthal directions from node 1. In Figure. 5.9, nodes 2, 3, 4 and 5 are located 2km, 5km, 6km and 7km, respectively, away from node 1. At each node the receiver may be located at different depths and node 4 has 2 different receiver elements.

The objective in this section is to illustrate the case where node 1 transmits simultaneously in time and frequency different message signals to each one of the receivers at the other nodes. In order to accomplish this, node 1 takes advantage of the spatial focusing diversity of PCA 1. In other words, PCA 1 is able to simultaneously focus different messages at different locations.

In a network environment, this technique can be difficult to implement. Each PCA has to record and store the received probe pulse from each one of the source/receiver elements at the other communication nodes. At each focusing stage only one probe pulse is sent by one of the source/receiver elements and will be recorded by the PCA's at the other communication nodes. At the end of the probing process PCA 1 will have stored the necessary signals to focus at all the receivers. For example, if PCA 1 wants to send a message to source/receiver nr. 5, it uses only the stored signals from source/receiver nr.5 probe signal to compose signals to be transmitted that will focus the desired message at the receiver 5 location. In the case where node 1 broadcasts a message for all receivers, PCA 1 will use all the signals recorded from each source/receiver probe pulse transmission to compose the signals that will be transmitted by each element.

Figure 5.10 represents the desired message signal spectrograms that node 1 wants to focus at each receiver of Figure 5.9. Note that these signals do not correspond to the actual signals sent by the PCA 1 elements. At each PCA 1 element the transmitted signal will include multipath and other channel distortions due to spatial variability of channel conditions. As seen in Figure. 5.10, four of the desired received signals only have one frequency component. The motivation behind this choice of message signals is to observe

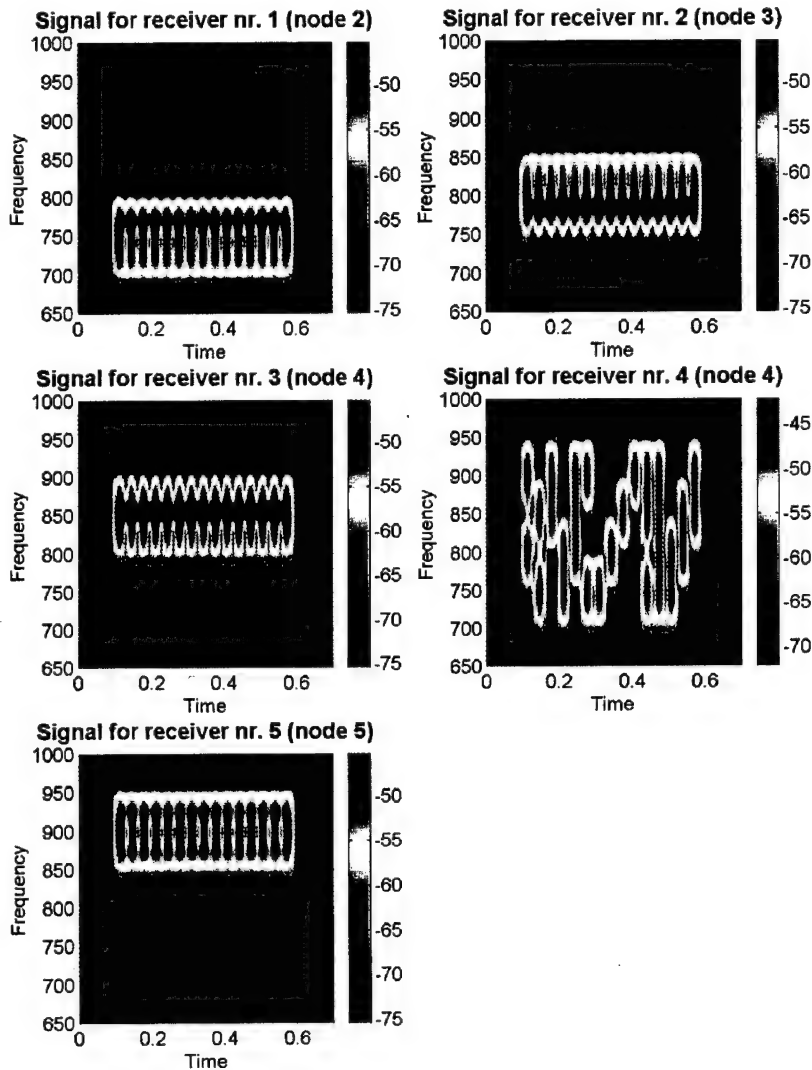


Figure 5.10. Desired Signals to Focus at the Receivers.

intersymbol interference due to temporal overlapping of the different transmitted messages.

Figure 5.11 represents numerical simulation results corresponding to the situation where node 1 transmits simultaneously the appropriate signals to focus each message of Figure 5.10 at the corresponding receiver. Again, in this simulation it was assumed that the node 1 PCA spans the entire water column. The results in Figure 5.11 show that little interference was attained and each receiver is able to decode the correct message.

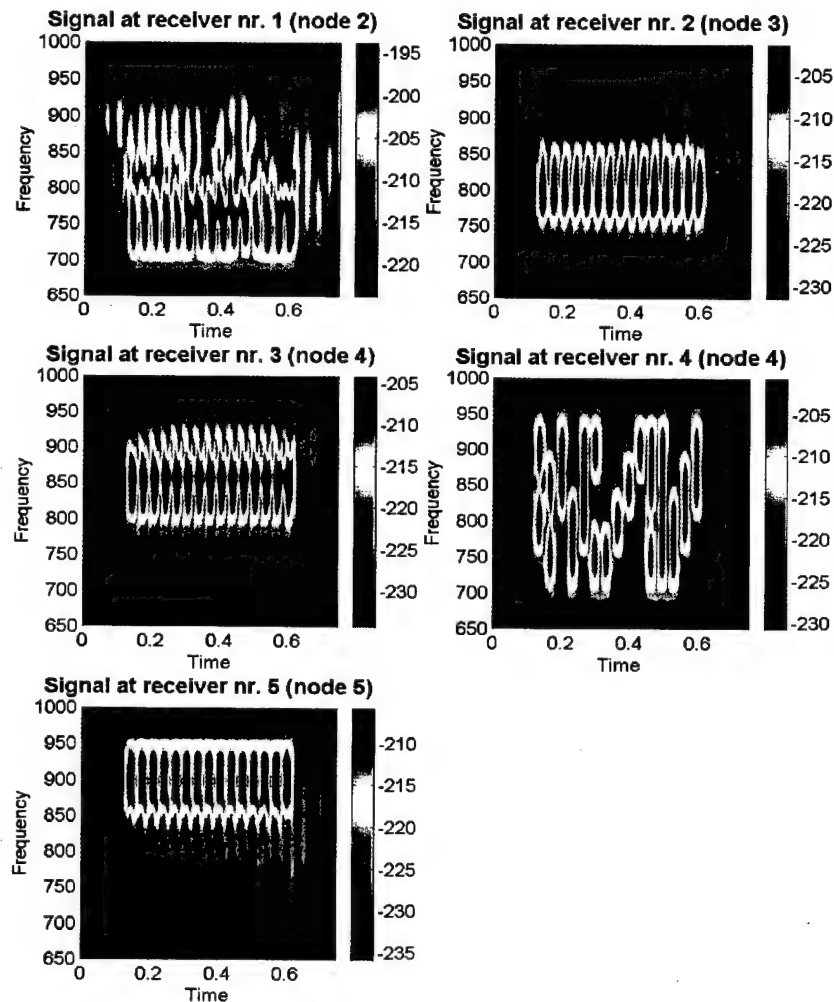


Figure 5.11. Received Signal Spectrogram at the Receivers.

Figure 5.12 represents the received signal spectrogram at different ranges between node 1 and node 2 collected at a depth of 150m. The results in this figure show that it will be extremely difficult to decode the original messages at these locations because the different message signals are overlapping both in time and frequency.

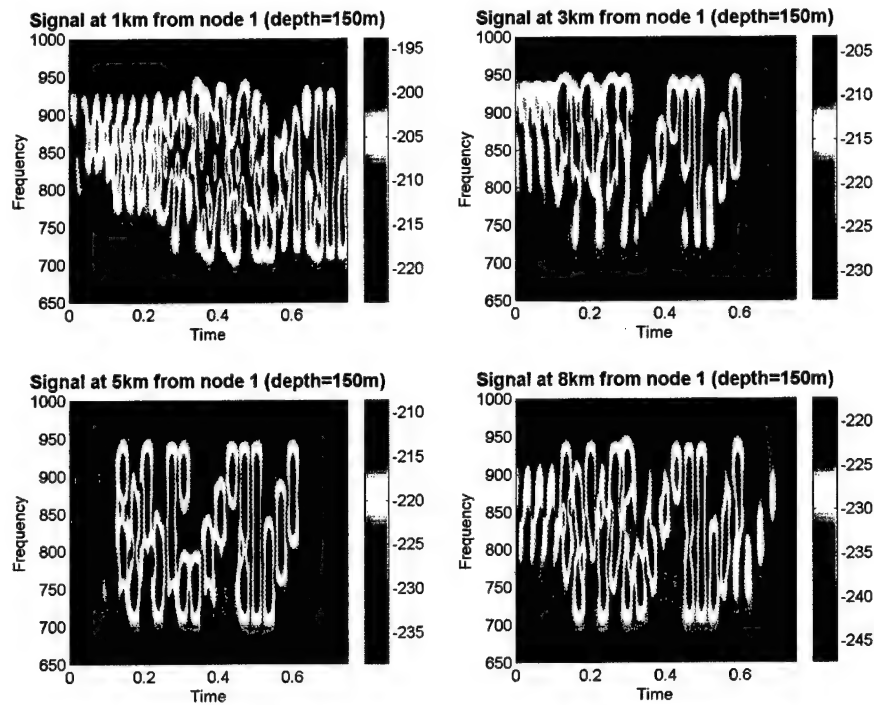


Figure 5.12. Received Signal Spectrogram at a Depth of 150m and Different Ranges from Node 1.



## VI. CONCLUSIONS

In this thesis an attempt was made to characterize the influences of a phase-conjugation array design on its focusing properties. Particular attention was given to PCA applications in UWA communication systems. This thesis provides a starting point for a PC array design, and gives support to the planning of further TRA UWA communication experiments both in the laboratory and in an oceanic environment. In the early stages of a TRA UWA communication system design, TRA numerical modeling is very important because it gives insight to the propagation issues that are involved without the need to go out to the ocean and perform very expensive experiments. However, although numerical modeling is an excellent analysis tool, it does not provide complete information about time-variability of the channel conditions. To take that into account and incorporate it in the UWA communication system design, oceanic experiments are planned for the near future.

The numerical analysis of the PCA focusing properties showed that the focus footprint decreases in dimensions as the carrier frequency increases. Furthermore, the horizontal dimension is larger than the vertical dimension of the footprint. Therefore vertical motion of the receiver is much more critical than horizontal motion because the receiver can easily move out-of-focus.

Using the same bandwidth and changing carrier frequency in the range 400Hz to 1200Hz, numerical modeling showed that temporal focusing does not change significantly. This is the case illustrated in Section 4.D with an effective pulse bandwidth of 36.6Hz. In a more general situation where a larger pulse bandwidth is used, the results in Figure 4.10 suggest that for carrier frequencies higher than 1200Hz, some degradation

will occur in the pulse temporal resolution at the focus location since the two-way channel frequency response will change considerably over the bandwidth.

Using PC arrays with different element spacing or with different aperture size, the PCA footprint did not appear to change its dimensions. Keeping constant the aperture size and changing the PCA element spacing, the temporal sidelobes remained approximately at the same level. As illustrated in Figure 4.11, temporal sidelobes 25dB below the main lobe can be attained with an element spacing of 6.6 wavelengths (in this case the aperture size is 100m, half of the channel depth).

Keeping constant the PCA element spacing and changing the aperture size, the vertical and horizontal footprint size did not appear to change significantly. A small improvement in horizontal sidelobes was observed in Figure 4.12 as the aperture length was increased. Figure 4.12 also showed that with PCA aperture sizes of  $2.5\lambda_c$  (7 transducers),  $5\lambda_c$  (13 transducers) and  $10\lambda_c$  (25 transducers), the temporal sidelobes remained at the same level with respect to the main lobe. A dramatic improvement in temporal sidelobes was observed when the aperture size increased to  $20\lambda_c$  (49 transducers) because the PCA was able to provide better spatial sampling of the lowest propagation modes. In other words, there was more spatial diversity in the PC array.

What can be concluded from these experiments is that aperture size plays a more significant role than the number of array elements in a PC array design. In the examples shown in Figures 4.11 and 4.12, the PC array with an aperture size of 100m and only 9 transducers had lower temporal sidelobes than the PC array with an aperture size of 37.5m and 49 transducers. The number of PCA transducers is a critical factor in PC array design because it will drive up the cost. Each PCA transducer has its own electronic circuitry

composed of receiver amplifiers, A/D and D/A converters, storage memory and transmitter. In general, underwater devices rely on batteries to operate their electronic systems and have severe constraints on the amount of power that can be used. Thus, for cost effectiveness one would be better off with a small number of array elements extended over a large aperture size.

Another interesting TRA property that was observed is the horizontal shifting of the footprint location when the PCA shifts the carrier frequency of the transmitted signal. At this point it seems that this property may be useful in a UWA communication system where the stations may be in motion or drifting. Its implementation requires further research because each PCA must sense the rate of relative motion in order to keep the focus at the receiver location. The relationship between the frequency shifting and range of focus shifting is also environmentally dependent.

For UWA communication systems using noncoherent detection, the use of PC arrays seems promising because there is no requirement of carrier phase tracking. The temporal focusing properties of the PCA overcomes the requirement of guard times between consecutive symbols to ensure that all the reverberation will vanish before each subsequent symbol is received avoiding intersymbol interference at the receiver. Thus some data rate improvement is made because the insertion of idle periods of time results in a reduction of the available data throughput. Array processing is no longer required because the PCA footprint is well defined at the receiver location.

As seen in Chapter V, the data throughput can be further improved by taking advantage of the PCA spatial diversity focusing properties. In the cases presented, the PCA was able to focus simultaneously different messages at different receiver locations. The message signal designated for a given receiver only focused at the intended receiver



location. At the receiver the corresponding message signal was compressed in time and space and had higher magnitude than the other interfering message signals. As a consequence, each message signal could only be decoded at the desired receiver. Furthermore, this seems to be a good technique for secure UWA communications because the different message signals will be overlapping both in time and frequency at other locations, making it difficult to recover any of the transmitted messages.

Due to the PC array spatial diversity focusing properties, PC arrays may have an important role in an acoustic local area network. Each array is able to simultaneously transmit different messages that will focus at the destination receiver node. Although the first protocols for acoustic local area networks have been proposed by Brandy and Catipovic (1994) and Talavage et al. (1994), the design of an acoustic local area network protocol that accommodates the learning step of the PCA's is still yet to be developed.

In order to achieve high-speed data transmission, the use of TRA bandwidth-efficient phase-coherent communications requires further research. Due to temporal variability of channel conditions, the first step towards the feasibility of TRA phase-coherent communications is the evaluation of the phase-stability (phase fluctuations) at the focus. Once accomplished, the receiver structure can be determined and an adaptive equalizer can be designed to accommodate temporal variability of the channel conditions.

At this point it seems clear that if the PCA learns every symbol in the code, the symbols will arrive with the correct phase information at the receiver. This has the downside that it will take much more time for the PCA to learn the environment and it requires enough storage for all of that information. It would be an advantage if the PCA only needed to learn the reference symbol and could then process the collected data in order to generate at the receiver location all the different symbols in the code.

## LIST OF REFERENCES

Abrantes, A. M. A., Smith, K. B. and Larraza, A., (1999) "Examination of time-reversal acoustics and applications to underwater communications," 137th Meeting of the Acoustical Society of America, Berlin, Germany.

Baggeroer, A., (1984) "Acoustic telemetry - An overview," *IEEE Journal of Oceanic Engineering*, OE-9, pp. 229-235.

Baggeroer, A. B., Kuperman, W. A., and Mikhalevsky, P. N., (1993) "An overview of matched field methods in ocean acoustics," *IEEE Journal of Oceanic Engineering*, Vol. 18, pp. 401-424.

Brandy, D.P. and Catipovic, J.A., (1994) "Adaptive multiuser detection for underwater acoustic channels," *IEEE Journal of Oceanic Engineering*, Vol. 19, pp. 158-165, Apr. 1994.

Brekhovskikh, L. M. and Lysanov, Y., (1991) *Fundamentals of Ocean Acoustics*, Springer-Verlag, Berlin, pp. 139-145.

Brienzo, R. K. and Hodgkiss, W. S., (1993) "Broadband matched-field processing," *Journal of the Acoustical Society of America*, Vol. 94, pp. 2821-2831.

Catipovic, J., (1990) "Performance limitations in underwater acoustic telemetry," *IEEE Journal of Oceanic Engineering*, Vol. 15, pp. 205-216.

Chin-Bing, S. A., King, D. B., Davis, J. A., and Evans, R. B., (1993) "Lloyd's Mirror - Wide Angle Propagation," *PE Workshop II: Proceedings of the Second Parabolic Equation Workshop*, Naval Research Laboratory NRL/BE/7181-93-0001 (US Government Printing Office, pp. 62-67.

Chuprov, S. D. and Mal'tsev, N. E., (1981) *Dolk. Akad. Nauk SSSR*, 257, pp. 475-479.

Chuprov, S. D., (1982) "Interference structure of a sound field in layered media," *Acoustics of the ocean: current status* (in Russian), edited by Brekhovskikh, L. M. and Andreevoi, I. B. (Nauka, Moscow), pp. 71-91.

Coates, R. F. W., (1993) "Underwater acoustic communications," *Proc. OCEANS'93*, Victoria, BC, pp. III.420-III.425.

Coates, R., Owens, R., and Tseng, M., (1993) "Underwater acoustic communications: A second bibliography and review," *Proc. Inst. Acoust.*

Feit, M. D. and Fleck, J. A., (1978) "Light propagation in graded-index fibers," *Appl. Opt.* 17, pp. 3990-3998.

Galvin, R. and Coates, R. F. W., (1994) "Analysis of the performance of an underwater acoustic communication system and comparison with a stochastic model," *Proc. OCEANS'94*, Brest, France, pp. III.478-III.482.

Grachev, G. A., (1993) "Theory of acoustic field invariants in layered waveguide," *Acoust. Phys.*, Vol. 39, pp. 33-35.

Gradshteyn, I. S. and Ryzhik, I. M., (1994) *Table of Integrals, Series and Products*, Academic Press, Inc., pp. 966 and 972.

Hardin, R.H. and Tappert, F.D., (1973) "Applications of the split-step Fourier method to the numerical solution of nonlinear and variable coefficient wave equations," *SIAM Rev.* 15, pp. 423.

Henderson, G. B., Tweedy, A., Howe, G. S., Hinton, O., and Adams, A. E., (1994) "Investigation of adaptive beamformer performance and experimental verification of applications in high data rate digital underwater communications," *Proc. OCEANS'94*, Brest, France, pp. I.296-I.301.

Howe, G. S., Tarbit, P., Hinton, O., Sharif, B., and Adams, A., (1994) "Sub-sea acoustic remote communications utilizing an adaptive receiving beamformer for multipath suppression," *Proc. OCEANS'94*, Brest, France, pp. I.313-I.316.

Jackson, D. R. and Dowling, D. R. (1991) "Phase conjugation in underwater acoustics," *Journal of the Acoustical Society of America*, Vol. 89, pp. 171-181.

Jensen, F. B., Kuperman, W. A., Porter M. B., and Schmidt H., (1994) *Computational Ocean Acoustics*, American Institute of Physics Press, Woodbury, NY.

Kuperman, W. A., Hodgkiss, W. S., Song, H. C., Akal, T., Ferla, C., and Jackson, D.R. (1998) "Phase conjugation in the ocean: Experimental demonstration of an acoustic time-reversal mirror," *Journal of the Acoustical Society of America*, Vol. 103, pp. 25-40.

Press, W. H., Flannery, B. P., Teukolsky, S. A., and Vetterling, W. T., (1988) *Numerical Recipes*, Cambridge University Press, New York, NY.

Proakis, J.G. and Manolakis, D.G., (1996) *Digital signal processing: principles, algorithms, and applications*, Prentice Hall, Upper Saddle River, NJ.

Smith, K.B. and Tappert F.D., (1994) "UMPE: The University of Miami Parabolic Equation Model, Version 1.1", MPL Technical Memorandum 432, 1993 (revised September 1994).

Smith, K. B., (1996) Personal communication, Naval Postgraduate School.

Song, H. C., Kuperman, W. A., and Hodkiss, W. S., (1998) "A time-reversal mirror with variable range focusing," *Journal of the Acoustical Society of America*, Vol. 103, pp. 3234-3240.

Stojanovic, M., Catipovic, J.A., and Proakis, J.G., (1993) "Adaptive multichannel combining and equalization for underwater acoustic communications," *Journal of the Acoustical Society of America*, Vol. 94, No. 3, pt. 1, pp.1621-1631.

Stojanovic, M., Catipovic, J.A., and Proakis, J.G., (1994) "Phase coherent digital communications for underwater acoustic channels," *IEEE Journal of Oceanic Engineering*, Vol. 19, pp. 100-111.

Stojanovic, M., Catipovic, J.A., and Proakis, J.G., (1995) "Reduced-complexity spatial and temporal processing of underwater acoustic communication signals," *Journal of the Acoustical Society of America*, Vol. 98, No. 2, pt. 1, pp.961-972.

Stojanovic, M., (1996) "Recent advances in high-speed underwater acoustic communications," *IEEE Journal of Oceanic Engineering*, Vol. 21, pp. 125-136.

Talavage, J., Thiel, T., and Brandy, D. (1994) "An efficient store-and-forward protocol for a shallow water acoustic local area network," *Proc. OCEANS'94*, Brest, France.

Tappert, F.D., (1974) "Parabolic equation method in underwater acoustics," *Journal of the Acoustical Society of America Suppl. 1*, Vol. 55, S34.

Tappert, F.D., (1977) "The parabolic approximation method," *Wave Propagation and Underwater Acoustics, Lecture Notes in Physics*, edited by J.B. Keller and J.S. Papadakis (Springer-Verlag, Berlin), Vol. 70, pp. 224-278.

Tarbit, P.S.D., Howe, G., Hinton, O., Adams, A., and Sharif, B., (1994) "Development of a real-time adaptive equalizer for a high-rate underwater acoustic data communication link," *Proc. OCEANS'94*, Brest, France, pp. I.307-I.312.

Thomson, D.J. and Chapman, N.R., (1983) "A wide-angle split-step algorithm for the parabolic equation," *Journal of the Acoustical Society of America*, Vol 74, pp. 1848-1854.



## INITIAL DISTRIBUTION LIST

1. Defense Technical Information Center .....2  
 8725 John J. Kingman Rd., STE 0944  
 Ft. Belvoir, VA 22060-6218
  
2. Dudley Knox Library .....2  
 Naval Postgraduate School  
 411 Dyer Rd.  
 Monterey, CA 93943-5101
  
3. Professor Kevin B. Smith .....5  
 Code PH/Sk  
 Physics Department  
 Naval Postgraduate School  
 Monterey, CA 93943-5117
  
4. Professor Andrés Larraza .....1  
 Code PH/La  
 Physics Department  
 Naval Postgraduate School  
 Monterey, CA 93943-5117
  
5. Chairman, .....1  
 Code EC  
 Department of Electrical and Computer Engineering  
 Naval Postgraduate School  
 Monterey, CA 93943-5101
  
6. Professor Monique P. Fargues .....1  
 Code EC/Fa  
 Department of Electrical and Computer Engineering  
 833 Dyer Rd., Rm. 437  
 Naval Postgraduate School  
 Monterey, CA 93943-5121
  
7. Direcção do Serviço de Formação - R.A.E. ....1  
 Edifício Administração Central de Marinha  
 Praça do Município  
 1188 Lisboa Codex  
 Portugal

8. LT António A. M. Abrantes .....	2
5200 Coe Ave., Apt. 1155	
Seaside, CA 93955	